IEEE Access
Multidisciplinary | Rapid Review | Open Access Journal

Received 23 November 2023, accepted 6 December 2023, date of publication 19 December 2023,
date of current version 8 January 2024.

Digital Object Identifier 10.1109/ACCESS.2023.3345250

RESEARCH ARTICLE

Fixed-Time Self-Structuring Neuron Network-Based Adjustable Prescribed Performance Control for a Quadrotor UAV With Input Saturation

HAITAO LIU[1,2], (Member, IEEE), HONGJI ZHENG[1,3], YUAN ZHANG[2,4], AND LIJIAO WEI[2,4]

[1]School of Mechanical Engineering, Guangdong Ocean University, Zhanjiang 524088, China
[2]Guangdong Engineering Technology Research Center of Ocean Equipment and Manufacturing, Zhanjiang 524088, China
[3]Agricultural Machinery Research Institute, Chinese Academy of Tropical Agricultural Sciences, Zhanjiang 524091, China
[4]GuangDong Engineering Technology Research Center of Precision Emission Control for Agricultural Particulates, Zhanjiang 524001, China

Corresponding author: Hongji Zheng (zhenghj28@126.com)

This work was supported in part by the Key Project of the Department of Education of Guangdong Province under Grant 2021ZDZX1041, in part by the Shenzhen Science and Technology Program under Grant JCYJ20220530162014033, in part by the Guangdong/Zhanjiang Engineering Technology Research Center of Precision Emission Control for Agricultural Particulates under Grant 2022A105, in part by the Zhanjiang Key Laboratory of Dynamics and Precision Emission Control for Particulates under Grant 2020A05004, in part by the Special Topic on Agricultural Research of Zhanjiang Science and Technology Plan Project under Grant 2021A05194, and in part by the Guangdong Provincial Enterprise Science and Technology Commissioner Project under Grant GDKTP2021008500.

ABSTRACT This paper introduces a fixed-time self-structuring neural network (SSNN)-based adjustable prescribed performance control for quadrotors designed to handle mutational external disturbances and input saturation. To address the unpredictable nature of such disturbances during missions, SSNN is proposed for limited on-board resources of the quadrotors. This kind of neural network can adaptively adjust the number of neurons in real time to achieve more precise estimations while minimizing resource consumption. Second, to overcome the singularity problem that arises when the tracking error may exceed the boundary of the envelope when a mutation disturbance occurs, an adaptively adjustable prescribed performance function is proposed to constrain the tracking error, which is always within the envelope to avoid the singularity problem. A fixed-time adaptive command filter that can estimate an unknown upper bound on the derivative of the virtual control law with respect to time is proposed and improves the convergence rate. Under Lyapunov's theorem, it is demonstrated that the closed-loop system can converge to the origin within a fixed time, showcasing the effectiveness of the proposed control strategy as evidenced by comparative simulation results.

INDEX TERMS Adjustable prescribed performance, self-structuring neuron network, fixed-time stability, input saturation, quadrotor UAV.

NOMENCLATURE

$\mathbf{p} = [x, y, z]^T$	position vector.
$\boldsymbol{v} = [v_x, v_y, v_z]^T$	Linear velocity vector.
$\boldsymbol{\Theta} = [\phi, \theta, \psi]^T$	Angle vector.
$\boldsymbol{\omega} = [\omega_\phi, \omega_\theta, \omega_\psi]^T$	Angular rate vector.
m	Total mass.
g	Gravity acceleration.
$\mathbf{J} = diag\{J_x, J_y, J_z\}$	Inertia matrix.
$d_v = [d_x, d_y, d_z]^T$	External disturbance in trajectory subsystem.
$d_\omega = [d_\phi, d_\theta, d_\psi]^T$	External disturbance in the attitude subsystem.
ω_i	Angular velocity of the i-th rotor.
b	Drag force coefficient.
l	Distance from the rotor to the center of mass.
c	The reverse moment coefficient.
J_r	Inertia moment of the rotor.

The associate editor coordinating the review of this manuscript and approving it for publication was Mohammad Alshabi.

I. INTRODUCTION

Recently, quadrotor unmanned aerial vehicles (UAVs) have found widespread employment in industrial and academic domains, demonstrating significant potential in areas such as agriculture, environmental reconnaissance, logistics and transportation, and disaster detection [1], [2], [3], [4]. Compared with fixed-wing and helicopter UAVs, quadrotor UAVs have a simple structure, convenient maintenance and excellent maneuverability. Even though the quadrotor offers all of these benefits, it is challenging to develop a reliable and robust controller because of the abovementioned factors [5], [6], [7], [8]. First, the quadrotor system is a complex dynamical system with six degrees of freedom (DOFs), characterized by underactuation, strong coupling, and nonlinearity. In addition, during actual flight, the quadrotor inevitably encounters environmental disturbances, including aerodynamic disturbances and wind gusts, which can destabilize the system due to its lightweight structure and motor output limitations. Therefore, it is essential to design a control scheme that is efficient and robust, taking into consideration the aforementioned factors simultaneously.

The majority of such schemes have commonly been based on a state feedback control strategy [9], [10], [11], [12], [13]. For example, a nonlinear implicit proportional-integral-derivative (PID)-type controller was implemented in a quadrotor system to obtain optimal feedback gains [9]. In [10], to address the inherent challenge of ''complexity explosion'' in backstepping design, a sigmoid tracking differentiator (STD) was employed to circumvent tedious analytical calculations, enabling the construction of a robust backstepping output feedback trajectory tracking controller. In [11], recursive sliding mode control (RSMC) was established to reduce chattering and guarantee a fast response. A unit quaternion-based model predictive control (MPC) technique was proposed for quadrotors, which can ascertain a smooth singularity-free flight within model uncertainty [12]. Nonetheless, the application of MPC for trajectory tracking in low-cost autopilots is challenging due to the substantial computational complexity and significant memory consumption involved. In [13], a special learning structure based on some approximation of back-propagation error that can be applied to adaptive control using neural networks was proposed. Although the designed antidisturbance controller for quadrotors can ultimately ensure uniformly bounded (UUB) results, its upper bound will be infinitely growing as the initial state tends to infinity because when the initial condition of the quadrotor is difficult to obtain accurately, the setting convergence time is unspecified in advance. In [14], Polyakov proposed the fixed-time stability method, which extends the concept of finite-time stability. This approach ensures convergence within a predetermined period that is independent of initial conditions, solely determined by the controller gain. In [15], a fault-tolerant tracking control strategy based on a disturbance observer and fixed-time sliding mode (FTSM) is proposed for a quadrotor system. In [16], an observer-based adaptive sliding mode control (SMC) strategy was proposed to achieve fixed-time stability for the attitude error system. Additionally, a sinusoidal function was employed as a nonlinear function to mitigate chattering and singularity issues in the control scheme. In [17], a nonsingular fast terminal sliding mode (NFTSMC) control strategy for quadrotors was proposed, and asymptotic stability of the tracking error was achieved. However, the convergence region of all closed-loop signals in the aforementioned strategies is reliant on the bounds of certain unknown terms. Most of the fixed-time control schemes for quadrotors could cause an unpredictable accident due to only considering the steady-state performance of the tracking error without transient performance. Prescribed performance control (PPC) methods [18], [19], [20], [21] are known for constraining the tracking error within a predefined function and have been extensively studied and widely employed in the literature. The PPC methods utilize an error transformation function to convert the constrained dynamics into unconstrained dynamics and integrate the original dynamics with performance functions. In [18], the tracking error signal of the closed-loop system can converge to within a prescribed performance boundary in a fixed time by using an adaptive fixed-time command filter and a fractional-power error compensation mechanism. In [19], to satisfy a 6-DOF spacecraft rendezvous and docking operation, a novel filter compensation system was proposed and combined with dynamic surface control (DSC) theory and a radial basis function neural network (RBF-NN) to ensure the performance constraints of all closed-loop states. To achieve global proximate tracking in the fixed-time stabilization of uncertain robot manipulators, a nonsingular terminal sliding mode PPC strategy is proposed in [20], which combines the advantages of fixed-time methods, sliding mode algorithms, and PPC, resulting in an improved convergence rate and steady-state and transient performance. To avoid the issue of singularity caused by the maximum value of the tracking error that may exceed the predefined performance boundary, an adjustable prescribed performance function (APPF) is proposed, and a new compensation system is designed for the input saturation problem for hypersonic flight vehicles that are subject to actuator saturations in [21]. In [22], A novel approximation-free simple control scheme is proposed, along with a thrust saturation approach, which is capable of bypassing ideal attitude extraction singularities in position control design. Considering the characteristics of quadrotor aircraft in practical applications (e.g., simple structure, strong coupling), it is inevitable that the system will be destabilized by external mutation disturbances such as wind gusts when performing missions in the air. In response to this problem, addressing the impact of external mutation disturbances on quadrotor systems will be the focus of our forthcoming research.

In addition to designing robust controllers, several solutions have been proposed to enhance the robustness and adaptiveness of quadrotor systems against unknown

disturbances [23], [24], [25], [26]. In [23], the authors proposed a disturbance observer (DO) to estimate uncertainties and external disturbances for quadrotors. In [24], a solution proposed is the utilization of an adaptive sliding mode disturbance observer (ASMDO) in conjunction with a nested adaptive structure. This approach allows for the estimation of disturbances without relying on prior knowledge of their upper bounds or derivatives, thereby enhancing the robustness and adaptiveness of the quadrotor system against unknown disturbances. In [25] and [26], the extended state observer (ESO) is employed as a key component, playing a crucial role in the quadrotor system. The ESO is utilized to expand the disturbance term of the system into a new state, allowing for estimation and compensation of uncertainties, thereby improving the robustness and adaptiveness of the quadrotor system against unknown disturbances. In [27] and [28], the uncertainty and disturbance estimator (UDE) is utilized to compensate for the modeling uncertainties and the unknown environmental disturbances, such that the formation errors converge asymptotically to zero. In addition to the methods mentioned above, fuzzy logic and neural networks (NNs) are also effective means of estimating nonlinear terms. In [29], an artificial neural network was utilized to approximate the unknown nonlinear term. In [30] and [31], by combining adaptive techniques and RBFNN, the estimated unknown nonlinear terms are made closer to the true value, and the robustness of the system is improved. Due to the characteristics of neural networks, more neurons represent a better approximation performance, but it is challenging to determine the optimal number of neurons.

Increasing the number of neurons will instead increase the computational burden of the system, which is unacceptable on a quadrotor with limited on-board resources. To reduce the computational burden, some NNs strategies that can adjust the number of neurons online are available, such as SEGRNN(self-evolving general regression) was developed that can modify its structure and its parameters online to achieve the control goals based on the environment [32], a self-structured neural network (SS-NN) with a variable structure is employed to approximate the unknown dynamics in the nonlinear system [33], [34]. This kind of neural network can adjust the number of neurons online while ensuring the approximation performance, which is more realistic for practical applications.

Inspired by the aforementioned studies and taking into account the challenges of model uncertainty, external disturbances, and input saturation in quadrotor systems. This controller integrates adjustable prescribed performance with an adaptive self-structuring neural network to achieve the convergence of the closed-loop system to the origin within a fixed time. The main innovations of the proposed controller can be summarized as follows:

(i) Different from the fixed-boundary envelope PPC [35], [36], [37], the proposed prescribed control can avoid the control singularity problem by readjusting the envelope boundary to achieve improved transient and steady-state tracking performance.

(ii) To cope with the ''Differential Explosion'' problem, which may be caused by the time derivatives of the virtual control law, we propose a kind of adaptive fixed-time command filter. Unlike [18], this method can estimate an unknown upper bound on the derivative of the virtual control law and enhance the stability of the closed-loop control system.

(iii) To address lump disturbances, including model uncertainties and external disturbances, self-structuring neural networks (SSNNs) are proposed. In contrast to RBF-NN [19], [30], [31]. SSNN allows for the online adjustment of neuron count based on compensation efficiency, resulting in more accurate approximation performance with fewer resource requirements.

The rest of this paper is structured as follows. Section II introduces the preliminaries. Section III presents the design of the control strategy and the detailed closed-loop system stability analysis. Section IV presents numerical simulations to verify the proposed method. Section V summarizes the whole article and prospects for future work.

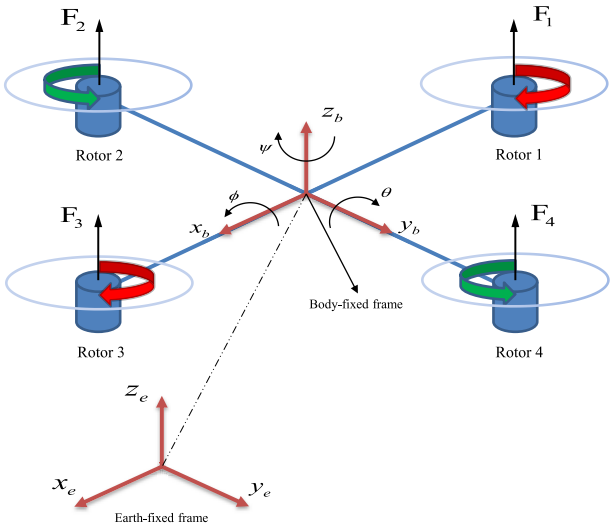

FIGURE 1. A simplified sketch of the structure of the quadrotor.

II. MODEL DESCRIPTION AND PRELIMINARIES

A. DYNAMICS SYSTEM DESCRIPTION

As illustrated in Fig. 1, an earth-fixed coordinate $\mathbf{E} = \{x_e, y_e, z_e\}$ and a body-fixed coordinate $\mathbf{B} = \{x_e, y_e, z_e\}$ are established, which simplifies the description of flight states. The dynamics of the quadrotor UAV model, considering parameter uncertainties, external disturbances, and input saturation, are described as [38].

$$\ddot{x} = sat\left(\tau_f\right)\left(\cos\phi\sin\theta\cos\psi + \sin\phi\sin\psi\right)/m - K_x\dot{x}/m + d_x$$
$$\ddot{y} = sat\left(\tau_f\right)\left(\cos\phi\sin\theta\sin\psi - \sin\phi\cos\psi\right)/m$$

$$
\begin{aligned}
&\quad - K_y\dot{y}/m + d_y \\
\ddot{z} &= sat\left(\tau_f\right)\left(\cos\phi\cos\theta\right)/m - g - K_z\dot{z}/m + d_z \\
\ddot{\phi} &= \dot{\theta}\dot{\psi}\frac{\left(J_y - J_z\right)}{J_x} - \frac{J_r}{J_x}\dot{\theta}\bar{\varpi} - \frac{K_\phi}{J_x}\dot{\phi} + \frac{1}{J_x}sat\left(\tau_\phi\right) + d_\phi \\
\ddot{\theta} &= \dot{\phi}\dot{\psi}\frac{\left(J_z - J_x\right)}{J_y} - \frac{J_r}{J_y}\dot{\phi}\bar{\varpi} - \frac{K_\theta}{J_y}\dot{\theta} + \frac{1}{J_y}sat\left(\tau_\theta\right) + d_\theta \\
\ddot{\psi} &= \dot{\phi}\dot{\theta}\frac{\left(J_x - J_y\right)}{J_z} - \frac{K_\psi}{J_z}\dot{\psi} + \frac{1}{J_z}sat\left(\tau_\psi\right) + d_\psi
\end{aligned} \tag{1}
$$

where $\bar{\varpi} = F_4 + F_3 - F_2 - F_1$ represents the overall residual rotor angle and is considered a bounded disturbance. The total lift τ_f and control input $\boldsymbol{\tau}_\omega = \left[\tau_\phi, \tau_\theta, \tau_\psi\right]^T$ related to the rotor thrust are defined as

$$
\begin{aligned}
\tau_f &= F_1 + F_2 + F_3 + F_4 = b\left(\omega_1^2 + \omega_2^2 + \omega_3^2 + \omega_4^2\right) \\
\tau_\phi &= lF_3 - lF_1 = lb\left(\omega_3^2 - \omega_1^2\right) \\
\tau_\theta &= lF_4 - lF_2 = lb\left(\omega_4^2 - \omega_2^2\right) \\
\tau_\psi &= c\left(-F_1 + F_2 - F_3 + F_4\right) = c\left(-\omega_1^2 + \omega_2^2 - \omega_3^2 + \omega_4^2\right)
\end{aligned} \tag{2}
$$

For simplification, (1) can be converted to the following forms:

$$
\begin{cases}
\dot{\mathbf{p}} = \mathbf{v} \\
\dot{\mathbf{v}} = \left(sat\left(\tau_{\mathrm{f}}\right)\boldsymbol{\Xi}/\mathrm{m} - \mathbf{g}\right) + \mathbf{f}_{\mathrm{v}}(\mathbf{v}) + \mathbf{d}_{\mathrm{v}} \\
\boldsymbol{\Theta} = \dot{\boldsymbol{\omega}} \\
\dot{\boldsymbol{\omega}} = \mathbf{J}^{-1}sat\left(\boldsymbol{\tau}_\omega\right) + \mathbf{f}_\omega(\boldsymbol{\omega}) + \mathbf{d}_\omega
\end{cases} \tag{3}
$$

where $\mathbf{g} = [0, 0, mg]^T$ denotes the gravity of the quadrotor, the coupling term $\boldsymbol{\Xi}(\boldsymbol{\Theta}) = [\Xi_x, \Xi_y, \Xi_z]^T$ with $\Xi_x = \left(\cos\phi\sin\theta\cos\psi + \sin\phi\sin\psi\right)/m$, $\Xi_y = \left(\cos\phi\sin\theta\sin\psi - \sin\phi\cos\psi\right)/m$, and $\Xi_z = \left(\cos\phi\cos\theta\right)/m$ is a vector derived from the transformation between rotational dynamics and translational dynamics. The model parameter uncertainties caused by aerodynamic coefficients in the position subsystem and attitude subsystem are represented by $\mathbf{f}_v(\mathbf{v}) = [f_x, f_y, f_z]^T$ with $f_x = -K_x\dot{x}/m$, $f_y = -K_y\dot{y}/m$, $f_z = -K_z\dot{z}/m$, and $\mathbf{f}_\omega(\boldsymbol{\omega}) = [f_\phi, f_\theta, f_\psi]^T$ with

$$
\begin{aligned}
f_\phi &= \dot{\theta}\dot{\psi}\frac{\left(J_y - J_z\right)}{J_x} - \frac{J_r}{J_x}\dot{\theta}\bar{\varpi} - \frac{K_\phi}{J_x}\dot{\phi}, \\
f_\theta &= \dot{\phi}\dot{\psi}\frac{\left(J_z - J_x\right)}{J_y} - \frac{J_r}{J_y}\dot{\phi}\bar{\varpi} - \frac{K_\theta}{J_y}\dot{\theta}, \quad \text{and} \\
f_\psi &= \dot{\phi}\dot{\theta}\frac{\left(J_x - J_y\right)}{J_z} - \frac{K_\psi}{J_z}\dot{\psi}, \quad \text{respectively,}
\end{aligned}
$$

$\mathbf{K}_p = [K_x, K_y, K_z]^T$ and $\mathbf{K}_a = [K_\phi, K_\theta, K_\psi]^T$. The input saturation constraint function $sat\left(*\right)$ of quadrotors can be expressed as follows:

$$
sat\left(\tau_\iota\right) = \begin{cases}
\tau_{\iota,\max} sign\left(\tau_\iota\right), & if \ \left|\tau_\iota\right| > \tau_{\iota,\max} \\
\tau_\iota, & else
\end{cases} \tag{4}
$$

where $\tau_\iota(\iota = f, \phi, \theta, \psi)$ represents the desired control input, regardless of input saturation. $\tau_{\iota,\max}$ is the maximum control authority, and the ι-th component can be provided by each rotor.

Assumption 1: The time derivatives of lumped disturbance $\mathbf{D}_p = [D_x, D_y, D_z]^T = \mathbf{f}_v(\mathbf{v}) + \mathbf{d}_v$, $\mathbf{D}_a = [D_\phi, D_\theta, D_\psi]^T = \mathbf{f}_\omega(\boldsymbol{\omega}) + \mathbf{d}_\omega$ are hypothesized to be upper bounded, and there exist unknown nonnegative constants $\bar{D}$, which satisfy $\max\left\{\left\|\dot{\mathbf{D}}_p\right\|, \left\|\dot{\mathbf{D}}_a\right\|\right\} \le \bar{D}$.

Assumption 2 [39]: $x_d^{(i)}, y_d^{(i)}, z_d^{(i)}, \phi_d^{(i)}, \theta_d^{(i)}, \psi_d^{(i)} \in L_\infty[0, \infty)$ for $i = 0, 1$, describe the desired positions and yaw angles, respectively, where (i) is the i-th order derivative of the variable. There exist nonnegative constants ξ_x, ξ_y and ξ_z that satisfy $\left|x_d^{(1)}\right| \le \xi_x$, $\left|y_d^{(1)}\right| \le \xi_y$, $\left|z_d^{(1)}\right| \le \xi_z < g$ for all $t \ge 0$ and $\xi_x^2 + \xi_y^2 < (g - \xi_z)^2$.

Assumption 3 [40]: To prevent the singularity problem, restrict the roll angle ϕ and pitch angle θ to $(-\pi/2, \pi/2)$, and constrain the yaw angle ψ to $(-\pi, \pi)$.

Remark 1: Based on the currently available research [39], Assumption 1 is a prerequisite for traditional observer design. During quadrotor flight, the position and attitude subsystems have limited control inputs due to the upper bound on the maximum output torque of the motor. Furthermore, the energy of other external disturbances, including turbulence, is finite and short in duration. Therefore, Assumption 1 is considered reasonable from an engineering perspective, i.e., the derivatives of the external disturbances $\mathbf{d}_v$ and $\mathbf{d}_\omega$ with respect to time have an unknown upper bound.

B. SELF-STRUCTURING NEURAL NETWORKS (SSNNs)

The RBFNN is frequently employed to approximate uncertain disturbances because of its excellent approximation performance. Although increasing the number of neurons in the RBFNN can improve its approximate performance, the computational burden of the system increases, and determining the optimal number of neurons becomes challenging. In order to reduce the computational burden, SSNN selectively deletes certain neurons in the network and retains only the most effective ones. This process eliminates ineffective neurons, aiming to achieve optimal performance approximation with minimal neuron usage. Additionally, when uncertain disturbances change, neurons can adjust in real time, and the estimated result of the external disturbance can be directly compensated to the controller.

A continuous function $f\left(x\right)$ estimated by the following formula is

$$
f\left(x\right) = \left(W^*\right)^T h\left(x\right) + \mu\left(x\right), \quad \forall x \in \Re \tag{5}
$$

where x is the state of $f\left(x\right)$, $\mu\left(x\right)$ is the SSNN approximation error satisfying $\left\|\mu\left(x\right)\right\| < \bar{\mu}$, $\bar{\mu}$ is an unknown nonnegative constant, and W^* represents the optimal weight matrix, which is defined as

$$
W^* = \arg\min\left\{\sup_{x\in\Re}\left|f\left(x\right) - \left(W^*\right)^T h\left(x\right)\right|\right\} \tag{6}
$$

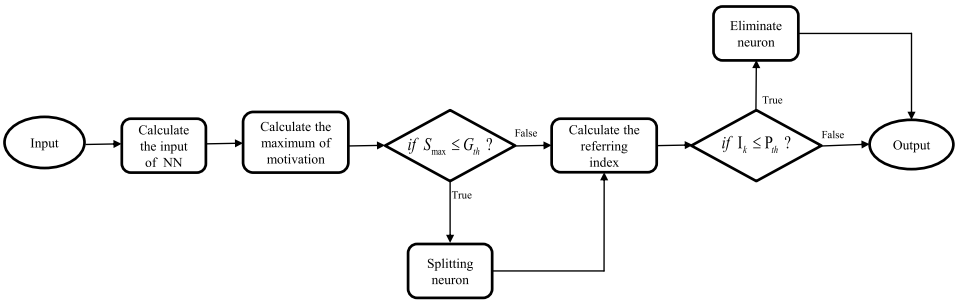

FIGURE 2. SSNN algorithm flowchart.

where $h(x)$ denotes the Gaussian basis function:

$$h_j(x) = \exp\left(-\frac{\|x - c_j\|^2}{2b_j^2}\right), \quad j = 1, 2, \ldots, N \tag{7}$$

where c_j and b_j represent the center vector of the j-th node in the hidden layer and the width of the Gaussian function $h_j(x)$, respectively.

The self-structuring strategy can be divided into two parts as follows:

(1) The neuron-splitting strategy is determined by comparing the splitting threshold $G_{th} \in (0, 1)$, which is the maximum value of activation of all neurons $h_{\max} = \max_{1 \le k \le s} h_k$, $k = 1, 2, \ldots, s$. If $h_{\max} \le G_{th}$, the neuron-splitting strategy is activated, i.e., the neurons do not achieve optimal activation, and a new neuron needs to be added to achieve a better effect. The update parameter of the new neuron is represented as follows:

$$\begin{cases} c_j^{new} = \dfrac{x_j + c_j}{2} \\ b_j^{new} = b_j \\ W_j^{new} = 0 \end{cases} \tag{8}$$

where c_j^{new} denotes the weight of the new neurons, x_j, c_j and b_j are the parameters of the maximum activated neurons, and W_j^{new} is the weight initial value of new neurons. A schematic diagram of the structural changes in neurons is shown in Fig 3.

(2) To avoid the computational overload caused by neuron overgeneration, eliminate the ineffective neurons. If the activation function h_k of the k-th neuron is below a preset delete threshold P_{th}, it suggests that the neuron may be underutilized or even inactive. By estimating the activation of this neuron, the neuron is finally removed if the culling strategy is satisfied, and the culling strategy is designed as follows:

$$I_k = \begin{cases} \exp(-\upsilon) I_k^p, & if\ h_k \le P_{th} \\ I_k^p, & if\ h_k > P_{th}, \end{cases} \qquad k = 1, 2, \ldots, N \tag{9}$$

where I_k denotes a censoring index. I_k^p represents the censoring index of the last recent calculation. The k-th neurons will be eliminated, which satisfies $I_k < I_{th}$. Adjusting the parameter value υ enables the neuron to perform multiple censoring judgments. The flow chart of the whole SSNN algorithm is presented in Fig. 2.

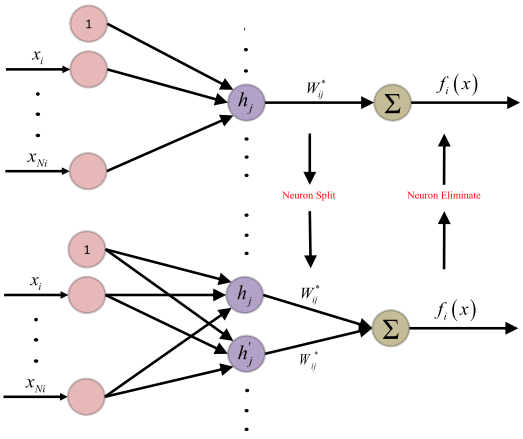

FIGURE 3. Structural diagram of neuronal changes.

Remark 2: If the unknown nonlinear system $f(x)$ approximated by the neural network is complex, a larger G_{th} is chosen, more neurons can be generated, and a better approximation can be achieved.

C. DEFINITIONS AND LEMMAS

Definition 1: Consider a nonlinear system as:

$$\dot{x}(t) = f(x), \quad x(0) = x_0 \tag{10}$$

where equation (10) achieves asymptotic stability; furthermore, if it achieves finite-time convergence, there exists a time T satisfying $\lim_{t \to T} x(t) = 0$ and $x(t) = 0$ for all $t \le T$.

Definition 2 [14]: The nonlinear system (10) is fixed-time stable if it is globally finite-time stable and the convergence time is bounded by the settling time $T(x_0) \in \Re$. Then, there exists a positive constant $T_{\max} \in \Re$ satisfying $T(x_0) \le T_{\max} \forall x_0$.

Lemma 1 [41]: If the given nonlinear system (10) satisfies the following inequality

$$\dot{V}(x) \le -\lambda_1 V(x)^{\alpha} - \lambda_2 V(x)^{\beta} + \ell \tag{11}$$

where $\lambda_1 > 0, \lambda_2 > 0, 0 < \alpha < 1, \beta > 1$ and $0 < \ell < \infty$.

Then, the fixed-time convergence time of the origin of the nonlinear system (10) is bounded by

$$T \leq \frac{1}{\lambda_1 \varpi (1-\alpha)} + \frac{1}{\lambda_2 \varpi (\beta - 1)} \tag{12}$$

where $0 < \varpi < 1$. The set of residuals for the solution of the nonlinear system yields the following results:

$$x \in \left\{ V(x) \leq \min \left\{ \left(\ell / (1-\varpi)\lambda_1\right)^{\frac{1}{\alpha}}, \left(\ell / (1-\varpi)\lambda_2\right)^{\frac{1}{\beta}} \right\} \right\} \tag{13}$$

Lemma 2 [42]: The following inequality satisfies any constant

$$0 < |\lambda| - \lambda \tanh\left(\frac{\lambda}{\partial}\right) < k\partial \tag{14}$$

where $\partial > 0$, $\lambda \in \Re$ and $k = 0.2785$.

Lemma 3 [43]: For any variables n, m and constants r, if $n > 0$, $m \geq 0$ and $r > 0$, satisfy the following inequality:

$$m^r (n-m) \leq \frac{1}{1+r}\left(n^{1+r} - m^{1+r}\right) \tag{15}$$

else if $n > 0$, $m \leq n$, and $r > 1$ satisfy

$$(m-n) \leq n^r - m^r \tag{16}$$

III. MAIN RESULTS

A. ADJUSTABLE PRESCRIBED PERFORMANCE

The trajectory tracking error of quadrotor dynamics is defined below:

$$\begin{cases} e_{p,1}(t) = p - p_d, \quad e_{p,2}(t) = v - z_p, \ p = x, y, z \\ e_{a,1}(t) = \Theta - \Theta_d, \quad e_{a,2}(t) = \omega - z_a, \ a = \phi, \theta, \psi \end{cases} \tag{17}$$

Inspired by [21], adjustable prescribed performance functions are proposed, which can be adaptively readjusted according to the input saturation to avoid the singularity problem.

First, in order to optimize the traditional prescribed performance function to reach a kind of adjustable prescribed performance function that can adjust the envelope curve in real time, the definition of an adjustable prescribed performance function is proposed as:

$$\rho_i = \left(\rho_0^i - \rho_\infty^i\right) exp(-\gamma_i t) + \rho_\infty^i + k_{1,i}(exp(k_{2,i}\delta_{u,i}) - 1) \tag{18}$$

where $\rho_\infty^i > \rho_0^i, k_{1,i} \in \Re^+ (i = x, y, z, \phi, \theta, \psi)$ and $k_{2,i} \in \Re^+$ are designed positive parameters, $\rho_i(0) = \rho_0^i$ indicates that the maximum overshoot in the transient phase should be less than ρ_0^i, $\rho_i(\infty) = \rho_\infty^i$ is utilized to constrain the tracking error in the steady-state phase, γ_i is the prescribed convergence rate for the tracking error. An auxiliary variable $\delta_{u,i\iota} = (f, \phi, \theta, \psi)$ is introduced to compensate for the input saturation as follows:

$$\dot{\delta}_{u,i} = -k_{s,1}\delta_{u,i} + k_{s,2} \min\{|\tau_\iota - sat(\tau_\iota)|\} \tag{19}$$

where $k_{s,1} \in \Re^+$ and $k_{s,2} \in \Re^+$ are positive design parameters.

To guarantee the tracking error $e_{i,1}(t)$ within boundary constraints of the states are as follows:

$$-\beta_i \rho_i(t) < e_{i,1}(t) < \bar{\beta}_i \rho_i(t) \tag{20}$$

where β_i and $\bar{\beta}_i$ are positive constants. The initial value of yield:

$$-\beta_i \rho_i(0) < e_{i,1}(0) < \bar{\beta}_i \rho_i(0) \tag{21}$$

Proposition 1: 1. $\zeta_i(\varepsilon_i)$ is a smooth and strictly increasing function;

2. $\lim_{\varepsilon_i \to -\infty} \zeta_i(\varepsilon_i) = \beta_i$ and $\lim_{\varepsilon_i \to \infty} \zeta_i(\varepsilon_i) = \bar{\beta}_i$;

3. where ε_i is a transformed error and the error $e_{i,1}$ is related to ε_i by

$$e_{i,1} = \rho_i \zeta_i(\varepsilon_i) \tag{22}$$

According to Proposition 1, an error transformation function that satisfies the above properties is chosen as follows:

$$\zeta_i(\varepsilon_i) = \frac{e_i(t)}{\rho_i(t)} = \frac{2}{\pi} \arctan(\varepsilon_i) \tag{23}$$

Then, the transformation function is introduced as follows:

$$\varepsilon_i = \zeta_i^{-1}\left(\frac{e_{i,1}(t)}{\rho_i(t)}\right) = \tan\left(\frac{\pi e_{i,1}(t)}{2\rho_i(t)}\right) \tag{24}$$

Taking the derivative of ε_i in (24)

$$\dot{\varepsilon}_i = r_i(\dot{e}_{i,1} + \lambda_i e_{i,1}) \tag{25}$$

where $r_i = \frac{\pi}{2\rho_i} \sec^2\left(\frac{\pi e_{i,1}}{2\rho_i}\right)$ and $\lambda_i = -\dot{\rho}_i/\rho_i$, $i = (x, y, z, \phi, \theta, \psi)$. When (21) is satisfied, we can obtain the inequality $r_i > \frac{\pi}{2\rho_i} > 0$ that holds.

Theorem 1: To maintain the initial constrained condition (21) for the tracking error, the prescribed performance envelope (20) can be implemented at any time interval, provided that the transformed tracking error $\varepsilon_i(t)$ remains bounded.

Remark 3: Since the traditional prescribed performance function cannot adjust the envelope boundary, thus causing the singularity problem, an adjustable prescribed performance function (18) is proposed, which can adjust the envelope boundary in real time to avoid the singularity problem in the case of mutation disturbances while guaranteeing that the transient and steady-state errors of the quadrotor system are stabilized within the error constraint boundary.

B. ADJUSTABLE PRESCRIBED PERFORMANCE FIXED-TIME CONTROLLER DESIGN

Next, a fixed-time prescribed performance controller is developed using the DSC strategy. This controller is designed to ensure that the trajectory tracking error converges to near zero

within a specified small region in a fixed time. The design process will be introduced in two steps.

Step 1: According to (25), the virtual control law $\mathbf{z}_{p,i} = [z_{p,x}, z_{p,y}, z_{p,z}]^T$ is derived as

$$\mathbf{z}_{p,i}(t) = \dot{\boldsymbol{p}}_d - \boldsymbol{e}_{p,1} - \boldsymbol{k}_{p,1}\boldsymbol{r}_p^{-1}\boldsymbol{\varepsilon}_p^{q_1} - \boldsymbol{k}_{p,2}\boldsymbol{r}_p^{-1}\boldsymbol{\varepsilon}_p^{q_2}. \quad (26)$$

where q_1, q_2 are designed positive constants and satisfy $0 < q_1 < 1$ and $1 < q_2$. $\boldsymbol{k}_{p,1}$ and $\boldsymbol{k}_{p,2}$ are diagonal matrices whose components are positive, $\boldsymbol{p}_d = [x_d, y_d, z_d]^T$, $\boldsymbol{e}_{p,1} = diag\{e_{x,1}, e_{y,1}, e_{z,1}\}$, $\boldsymbol{r}_p = diag\{r_x, r_y, r_z\}$, $\boldsymbol{\lambda}_p = [\lambda_x, \lambda_y, \lambda_z]^T$ and $\boldsymbol{\varepsilon}_p = [\varepsilon_x, \varepsilon_y, \varepsilon_z]^T$.

Assumption 4: The derivatives of the input signal of the filter $\dot{z}_i$ are continuous. There exist unknown nonnegative constants η_i that satisfy $|\dot{z}_i| \le \eta_i$

To avoid the "Differential Explosion" problems caused by the analytical derivative of calculation, an adaptive fixed-time command filter is designed as:

$$\begin{aligned} T_i\dot{\hat{z}}_i &= \xi_i^{q_m} + \xi_i^{q_n} + T_i\hat{\eta}_i \tanh\left(\frac{\xi_i\hat{\eta}}{\sigma_i}\right) \\ \dot{\hat{\eta}}_i &= -p_{i,1}\hat{\eta}_i^{q_m} - p_{i,2}\hat{\eta}_i^{q_n} + |\xi_i| \end{aligned} \quad (27)$$

where $\hat{z}_i i = (x, y, z, \phi, \theta, \psi)$ is the output of the filter, and $\hat{z}_i(0) = \hat{z}_i(0)$ is satisfied. where $0 < q_m < 1$, $1 < q_n, p_{i,1}$, $p_{i,2}$ and $\sigma_i > 0$ are designed as positive constants, which represent the gain of the filter and adaptive law, respectively. T_i denotes the time delay constant.

From Assumption 4, $\hat{\eta}_i$ is the estimate of η_i, and the error of the boundary estimated is defined as:

$$\tilde{\eta}_i = \eta_i - \hat{\eta}_i \quad (28)$$

The filtering error ξ_i generated by DSC is defined as:

$$\xi_i = z_i - \hat{z}_i \quad (29)$$

Construct the Lyapunov function V_f as follows:

$$V_f = \frac{1}{2}\boldsymbol{\xi}_p^T\boldsymbol{\xi}_p + \frac{1}{2}\boldsymbol{\xi}_a^T\boldsymbol{\xi}_a + \frac{1}{2}\tilde{\boldsymbol{\eta}}_p^T\tilde{\boldsymbol{\eta}}_p + \frac{1}{2}\tilde{\boldsymbol{\eta}}_a^T\tilde{\boldsymbol{\eta}}_a \quad (30)$$

Based on Lemma 2, differentiating V_f with respect to time yields

$$\begin{aligned} \dot{V}_f &= \boldsymbol{\xi}_p^T\dot{\boldsymbol{\xi}}_p + \tilde{\boldsymbol{\eta}}_p^T\dot{\tilde{\boldsymbol{\eta}}}_p + \boldsymbol{\xi}_a^T\dot{\boldsymbol{\xi}}_a + \tilde{\boldsymbol{\eta}}_a^T\dot{\tilde{\boldsymbol{\eta}}}_a \\ &\le -\frac{1}{T_p}\left(\boldsymbol{\xi}_p^T\boldsymbol{\xi}_p\right)^{\frac{1+q_m}{2}} - \frac{1}{T_p}\left(\boldsymbol{\xi}_p^T\boldsymbol{\xi}_p\right)^{\frac{1+q_n}{2}} - \frac{1}{T_a}\left(\boldsymbol{\xi}_a^T\boldsymbol{\xi}_a\right)^{\frac{1+q_m}{2}} \\ &\quad - \frac{1}{T_a}\left(\boldsymbol{\xi}_a^T\boldsymbol{\xi}_a\right)^{\frac{1+q_n}{2}} + k\left(\sigma_p + \sigma_a\right) + \left|\boldsymbol{\xi}_p^T\right|\tilde{\boldsymbol{\eta}}_p + \left|\boldsymbol{\xi}_a^T\right|\tilde{\boldsymbol{\eta}}_a \\ &\quad + \tilde{\boldsymbol{\eta}}_p^T\dot{\tilde{\boldsymbol{\eta}}}_p + \tilde{\boldsymbol{\eta}}_a^T\dot{\tilde{\boldsymbol{\eta}}}_a \end{aligned} \quad (31)$$

where $k = 0.2785$. By recalling Lemma 3, one has

$$\begin{aligned} \tilde{\eta}_p^T\hat{\eta}_p^{q_m} &\le \frac{1}{1+q_m}\left(2\eta_p^{1+q_m} - \tilde{\eta}_p^{1+q_m}\right) \\ \tilde{\eta}_p^T\hat{\eta}_p^{q_n} &\le \frac{1}{1+q_n}\left(2\eta_p^{1+q_n} - \tilde{\eta}_p^{1+q_n}\right) \\ \tilde{\eta}_a^T\hat{\eta}_a^{q_m} &\le \frac{1}{1+q_m}\left(2\eta_a^{1+q_m} - \tilde{\eta}_a^{1+q_m}\right) \\ \tilde{\eta}_a^T\hat{\eta}_a^{q_n} &\le \frac{1}{1+q_n}\left(2\eta_a^{1+q_n} - \tilde{\eta}_a^{1+q_n}\right) \end{aligned} \quad (32)$$

Then, substituting (27) into (31) and considering(32), we obtain

$$\dot{V}_f \le -k_{f_1}V_f^{m_t} - k_{f_2}V_f^{n_t} + c_f \quad (33)$$

where $m_t = \frac{1+q_m}{2}$, $n_t = \frac{1+q_n}{2}$, $k_{f_1} = \min\left\{\frac{1}{T_p}, \frac{1}{T_a}, \frac{p_{p,1}}{1+q_m}\right\}$,

$$\begin{aligned} k_{f_2} &= \min\left\{\frac{1}{T_p}, \frac{1}{T_a}, \frac{p_{p,2}}{1+q_n}\right\} \\ c_f &= \frac{2p_{p,1}}{1+q_m}\left(\eta_p^2\right)^{\frac{1+q_m}{2}} + \frac{2p_{p,2}}{1+q_n}\left(\eta_p^2\right)^{\frac{1+q_n}{2}} \\ &\quad + \frac{2p_{a,1}}{1+q_m}\left(\eta_a^2\right)^{\frac{1+q_m}{2}} \\ &\quad + \frac{2p_{a,2}}{1+q_n}\left(\eta_a^2\right)^{\frac{1+q_n}{2}} + k\left(\sigma_p + \sigma_a\right) \end{aligned}$$

Solving (33) results in $V_f(t) = 0$ when t holds $t \ge T_f$, and it is apparent that all filter signals will converge into the following region:

$$x \in \left\{V(x) \le \min\left\{\left(\frac{c_f}{(1-\varpi)k_{f_1}}\right)^{\frac{1}{m_t}}, \left(\frac{c_f}{(1-\varpi)k_{f_2}}\right)^{\frac{1}{n_t}}\right\}\right\} \quad (34)$$

In fixed time

$$T_f \le \frac{1}{k_{f_1}\varpi(1-m_t)} + \frac{1}{k_{f_2}\varpi(n_t-1)} \quad (35)$$

Remark 4: In contrast to [18], by utilizing the adaptive law, this method can estimate an unknown upper bound on the derivative of the virtual control law and enhance the stability of the closed-loop control system

Let $\dot{z}_p(t)$ pass through the fixed-time command filter(27), the position velocity tracking error be denoted as $\mathbf{e}_{p,2}(t) = \boldsymbol{v} - z_p$, and take the time derivative of $\mathbf{e}_{p,2}$ as follows:

$$\dot{\boldsymbol{e}}_{p,2} = \boldsymbol{u}_p + \boldsymbol{D}_p - \dot{\boldsymbol{z}}_p \quad (36)$$

According to [38], the dynamics of a quadrotor are a coupled and underactuated nonlinear system, implying that the position and attitude states cannot be controlled independently. To stabilize the linear velocity tracking error $\mathbf{e}_{p,2}$, the desired attitude angle $\boldsymbol{\Theta}_d = [\Theta_\phi^d, \Theta_\theta^d, \Theta_\psi^d]^T$ and its associated virtual control law $\boldsymbol{u}_p = [u_x, u_y, u_z]^T$ are designed as follows:

$$\begin{cases} u_x = (\cos\phi_d \sin\theta_d \cos\psi_d + \sin\phi_d \sin\psi_d)\tau_f/m \\ u_y = (\cos\phi_d \sin\theta_d \sin\psi_d - \sin\phi_d \cos\psi_d)\tau_f/m \\ u_z = (\cos\phi_d \cos\theta_d)\tau_f/m - g \end{cases} \quad (37)$$

Subsequently, taking the inverse transformation of (37), the total thrust τ_f, reference roll angle ϕ_d, and reference pitch angle θ_d can be derived as

$$\begin{cases} \tau_f = m\sqrt{u_x^2 + u_y^2 + (u_z + g)^2} \\ \phi_d = \arcsin\left[(u_x \sin\psi_d - u_y \cos\psi_d)m/\tau_f\right] \\ \theta_d = \arctan\left[(u_x \cos\psi_d + u_y \cos\psi_d)/(u_z + g)\right] \end{cases} \tag{38}$$

where the reference yaw angle ψ_d is assigned by a guidance level. To maintain the position subsystem state and achieve fixed-time convergence, the dynamic inversion principle is applied, and the virtual control input $\boldsymbol{u_p}$ is designed as follows:

$$\boldsymbol{u_p} = \dot{\hat{z}}_p - \boldsymbol{r}_p \boldsymbol{\varepsilon}_p - \hat{\mathbf{D}}_p - \boldsymbol{k}_{p,3}\boldsymbol{e}_{p,2}^{q_3} - \boldsymbol{k}_{p,4}\boldsymbol{e}_{p,2}^{q_4} \tag{39}$$

where $\boldsymbol{k}_{p,3}$ and $\boldsymbol{k}_{p,4}$ are diagonal matrices whose components have positive gains for the position subsystem, and q_3, q_4 are designed positive constants and satisfy $0 < q_3 < 1$, $1 < q_4$.

By recalling Assumption 1, $\hat{\mathbf{D}}_p = [\hat{D}_x, \hat{D}_y, \hat{D}_z]^T$ is the estimated value of $\mathbf{D}_p$.

Step 2: Define the attitude angle tracking error as $\boldsymbol{e}_{a,1}(t) = [e_{\phi,1}, e_{\theta,1}, e_{\psi,1}]^T = \boldsymbol{\Theta}(t) - \boldsymbol{\Theta}_d(t)$, and the time derivative of $e_{a,1}$ can be obtained as

$$\dot{\boldsymbol{e}}_{a,1} = \dot{\boldsymbol{\Theta}} - \dot{\boldsymbol{\Theta}}_d \tag{40}$$

To realize the tracking of the attitude angle in fixed time stabilization, the following virtual control law is established:

$$z_a(t) = \dot{\boldsymbol{\Theta}}_d - \boldsymbol{e}_{a,1} - \boldsymbol{k}_{a,1}\boldsymbol{r}_a^{-1}\boldsymbol{\varepsilon}_a^{q_1} - \boldsymbol{k}_{a,2}\boldsymbol{r}_a^{-1}\boldsymbol{\varepsilon}_a^{q_2} \tag{41}$$

where $\boldsymbol{k}_{a,1} = diag\left\{k_{\phi,1}, k_{\theta,1}, k_{\psi,1}\right\}$ and $\boldsymbol{k}_{a,2} = diag\left\{k_{\phi,2}, k_{\theta,2}, k_{\psi,2}\right\}$ denote the positive gain to be regulated, $\boldsymbol{e}_{a,1} = diag\{e_{\phi,1}, e_{\theta,1}, e_{\psi,1}\}$, $\boldsymbol{r}_a = diag\{r_\phi, r_\theta, r_\psi\}$, $\bar{\boldsymbol{\lambda}}_a = [\bar{\lambda}_\phi, \bar{\lambda}_\theta, \bar{\lambda}_\psi]^T$ and $\boldsymbol{\varepsilon}_a = [\varepsilon_\phi, \varepsilon_\theta, \varepsilon_\psi]^T$. Then, a filtered vector $\hat{\boldsymbol{z}}_a(t) = [\hat{z}_\phi, \hat{z}_\theta, \hat{z}_\psi]^T$ can be obtained by letting $\boldsymbol{z}_a(t)$ pass through the fixed-time command filter and define the angular velocity error $\boldsymbol{e}_{a,2}(t) = \left[e_{\phi,2}, e_{\theta,2}, e_{\psi,2}\right]^T = \boldsymbol{\omega} - \boldsymbol{z}_a$, whose differential in terms of time is derived as

$$\dot{\boldsymbol{e}}_{a,2} = \mathbf{J}^{-1}\boldsymbol{\tau}_\omega + \mathbf{D}_a - \dot{\boldsymbol{z}}_a \tag{42}$$

Based on (42), the practical torque action for the angular rates subsystem is designed as

$$\boldsymbol{\tau}_{\boldsymbol{\omega}} = \mathbf{J}\left(\dot{\hat{\boldsymbol{z}}}_a - \boldsymbol{r}_a\boldsymbol{\varepsilon}_a - \hat{\mathbf{D}}_a - \boldsymbol{k}_{a,3}\boldsymbol{e}_{a,2}^{q_3} - \boldsymbol{k}_{a,4}\boldsymbol{e}_{a,2}^{q_4}\right) \tag{43}$$

where $\boldsymbol{k}_{a,3} = diag\left\{k_{\phi,3}, k_{\theta,3}, k_{\psi,3}\right\}$ and $\boldsymbol{k}_{a,4} = diag\left\{k_{\phi,4}, k_{\theta,4}, k_{\psi,4}\right\}$ are the tunable nonnegative gain vectors for the attitude subsystem and $\hat{\boldsymbol{D}}_a = [\hat{D}_\phi, \hat{D}_\theta, \hat{\mathbf{D}}_\psi]^T$ is the estimated value of $\mathbf{D}_a$.

C. FIXED-TIME ADAPTIVE SS-NN-BASED ADJUSTABLE PRESCRIBED PERFORMANCE CONTROL STRATEGY DESIGN

As illustrated in Fig. 4, a fixed-time SS-NN-based adjustable prescribed performance control method is established with

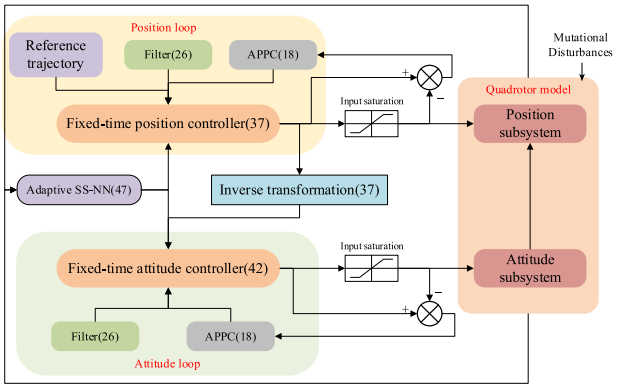

FIGURE 4. Block diagram of the proposed control.

input saturation, model uncertainties and mutational disturbances. The SS-NN-based strategy is employed with convergence for lump disturbances in a fixed time. The adaptive network weights $\hat{W}$ are constructed to estimate the desired weights W^* and the error matrix of the weight $\tilde{W} = W^* - \hat{W}$ is defined.

For simplicity of subsequent proofs, (1) is rewritten as follows:

$$\begin{cases} \dot{\mathbf{p}} = \mathbf{v} \\ \dot{\mathbf{v}} = \mathbf{u}_v + \mathbf{D}_p \\ \dot{\boldsymbol{\Theta}} = \boldsymbol{\omega} \\ \dot{\boldsymbol{\omega}} = \mathbf{J}^{-1}\boldsymbol{\tau}_\omega + \mathbf{D}_a \end{cases} \tag{44}$$

where $\mathbf{D}_p = \mathbf{f}_v(\mathbf{v}) + \mathbf{d}_v$ and $\mathbf{D}_a = \mathbf{f}_\omega(\boldsymbol{\omega}) + \mathbf{d}_\omega$. By recalling(5), we obtain

$$\begin{cases} \hat{\mathbf{D}}_p = \left(\boldsymbol{W}_p^*\right)^T \boldsymbol{h}_1\left(\boldsymbol{Z}_p\right) + \mu_p\left(\boldsymbol{Z}_p\right) \\ \hat{\mathbf{D}}_a = \left(\boldsymbol{W}_a^*\right)^T \boldsymbol{h}_2\left(\boldsymbol{Z}_a\right) + \mu_a\left(\boldsymbol{Z}_a\right) \end{cases} \tag{45}$$

where $\hat{\mathbf{D}}_p = \left[\hat{D}_x, \hat{D}_y, \hat{D}_z\right]^T$ and $\hat{\boldsymbol{D}}_a == \left[\hat{D}_\phi, \hat{D}_\theta, \hat{D}_\psi\right]^T$ represent the position and attitude system estimation of lumped disturbances, respectively. $\boldsymbol{Z}_v = \left[\boldsymbol{e}_{p,1}^T, \boldsymbol{e}_{p,2}^T\right]$ and $\boldsymbol{Z}_\omega = \left[\boldsymbol{e}_{a,1}^T, \boldsymbol{e}_{a,2}^T\right]$ are input vectors, and $\boldsymbol{W}_p^*$ and $\boldsymbol{W}_a^*$ are defined as (6).

The estimation error is calculated as

$$\tilde{\bar{\mu}}_i = \bar{\mu}_i - \hat{\bar{\mu}}_i \tag{46}$$

where μ_i indicates the approximation errors, $\|\mu_i(x)\| < \bar{\mu}_i$, and $i = x, y, z, \phi, \theta, \psi$.

Theorem 2: Under the conditions that the initial condition of APPF in (21) satisfies Assumptions 1-3 and the adaptive fixed-time command filter (27), the fixed-time controller (47), SS-NN adaptive law (48), and adaptive function (49) are utilized to guarantee that the tracking errors $e_{p,1}$ and $e_{a,1}$ converge within a fixed time to a neighborhood of the original subject to the performance constraint of the APPF, model uncertainties, input saturation and mutational

disturbances.

$$\begin{cases} \boldsymbol{u_p} = \dot{\hat{\boldsymbol{z}}}_p - \boldsymbol{\varepsilon_p r_p} - \hat{\boldsymbol{W}}_p^{\boldsymbol{T}} \boldsymbol{h}_1 (\boldsymbol{Z}_p) - \hat{\tilde{\boldsymbol{\mu}}}_p \tanh\left(\dfrac{\boldsymbol{e}_{p,2}}{\Upsilon_1}\right) \\ \quad -\boldsymbol{k_{p,3}} \boldsymbol{e}_{p,2}^{q_3} - \boldsymbol{k_{p,4}} \boldsymbol{e}_{p,2}^{q_4} \\ \boldsymbol{\tau}_\omega = \boldsymbol{J}(\dot{\hat{\boldsymbol{z}}}_a - \boldsymbol{\varepsilon}_a \boldsymbol{r}_a - \hat{\boldsymbol{W}}_a^{\boldsymbol{T}} \boldsymbol{h}_2 (\boldsymbol{Z}_a) - \hat{\tilde{\boldsymbol{\mu}}}_a \tanh\left(\dfrac{\boldsymbol{e}_{a,2}}{\Upsilon_2}\right) \\ \quad -\boldsymbol{k}_{a,3} \boldsymbol{e}_{a,2}^{q_3} - \boldsymbol{k}_{a,4} \boldsymbol{e}_{a,2}^{q_4}) \end{cases} \tag{47}$$

$$\begin{cases} \dot{\hat{\boldsymbol{W}}}_p = k_{w1} \left(\boldsymbol{h}_1(\boldsymbol{Z}_p) \boldsymbol{e}_{p,2}^T - k_{w2} \hat{\boldsymbol{W}}_p \right) \\ \dot{\hat{\boldsymbol{W}}}_a = k_{w3} \left(\boldsymbol{h}_2(\boldsymbol{Z}_a) \boldsymbol{e}_{a,2}^T - k_{w4} \hat{\boldsymbol{W}}_a \right) \end{cases} \tag{48}$$

where $\hat{\boldsymbol{W}}_i$ is the estimate of $\boldsymbol{W}_i^*$ and $k_{w1}, k_{w2}, k_{w3}, k_{w4}, \Upsilon_1, \Upsilon_2$ are nonnegative constants.

The adaptive law can be expressed as

$$\begin{cases} \dot{\hat{\tilde{\boldsymbol{\mu}}}}_p = k_{\mu 1} \left(\tanh\left(\dfrac{\boldsymbol{e}_{p,2}}{\Upsilon_1}\right) \boldsymbol{e}_{p,2} - k_{p,5} \hat{\tilde{\boldsymbol{\mu}}}_p^{q_5} - k_{p,6} \hat{\tilde{\boldsymbol{\mu}}}_p^{q_6} \right) \\ \dot{\hat{\tilde{\boldsymbol{\mu}}}}_a = k_{\mu 2} \left(\tanh\left(\dfrac{\boldsymbol{e}_{a,2}}{\Upsilon_2}\right) \boldsymbol{e}_{a,2} - k_{a,5} \hat{\tilde{\boldsymbol{\mu}}}_a^{q_5} - k_{a,6} \hat{\tilde{\boldsymbol{\mu}}}_a^{q_6} \right) \end{cases} \tag{49}$$

where $k_{\mu 1}$, $k_{\mu 2}$, $k_{p,5}$, $k_{p,6}k_{a,5}$, and $k_{a,6}$ are designed nonnegative gains.

Proof: To prove Theorem 2, construct a Lyapunov function V_1 as follows:

$$V_1 = \frac{1}{2} \boldsymbol{\varepsilon}_p^T \boldsymbol{\varepsilon}_p + \frac{1}{2} \boldsymbol{\varepsilon}_a^T \boldsymbol{\varepsilon}_a + \frac{1}{2} \boldsymbol{e}_{p,2}^T \boldsymbol{e}_{p,2} + \frac{1}{2} \boldsymbol{e}_{a,2}^T \boldsymbol{e}_{a,2} \tag{50}$$

Differentiating (50) with respect to time as follows

$$\dot{V}_1 = \boldsymbol{\varepsilon}_p^T \dot{\boldsymbol{\varepsilon}}_p + \boldsymbol{e}_{p,2}^T \dot{\boldsymbol{e}}_{p,2} + \boldsymbol{\varepsilon}_a^T \dot{\boldsymbol{\varepsilon}}_a + \boldsymbol{e}_{a,2}^T \dot{\boldsymbol{e}}_{a,2} \tag{51}$$

Substituting Eqs. (26), (41), and (47) into (51) yields

$$\begin{aligned} \dot{V}_1 \leq & -\boldsymbol{k}_{p,1} \left(\boldsymbol{\varepsilon}_p^2\right)^{\frac{1+q_1}{2}} \\ & - \boldsymbol{k}_{p,2} \left(\boldsymbol{\varepsilon}_p^2\right)^{\frac{1+q_2}{2}} - \boldsymbol{k}_{a,1} \left(\boldsymbol{\varepsilon}_a^2\right)^{\frac{1+q_1}{2}} - \boldsymbol{k}_{a,2} \left(\boldsymbol{\varepsilon}_a^2\right)^{\frac{1+q_2}{2}} \\ & - \boldsymbol{k}_{p,3} \left(\boldsymbol{e}_{p,2}^2\right)^{\frac{1+q_3}{2}} - \boldsymbol{k}_{p,4} \left(\boldsymbol{e}_{p,2}^2\right)^{\frac{1+q_4}{2}} - \boldsymbol{k}_{a,3} \left(\boldsymbol{e}_{a,2}^2\right)^{\frac{1+q_3}{2}} \\ & - \boldsymbol{k}_{a,4} \left(\boldsymbol{e}_{a,2}^2\right)^{\frac{1+q_4}{2}} + \boldsymbol{e}_{p,2}^T \tilde{\boldsymbol{W}}_p^{\boldsymbol{T}} h_1 (\boldsymbol{Z}_p) + \boldsymbol{e}_{a,2}^T \tilde{\boldsymbol{W}}_a^{\boldsymbol{T}} h_2 (\boldsymbol{Z}_a) \\ & - \boldsymbol{e}_{p,2}^T \hat{\tilde{\mu}}_p \tanh\left(\frac{\boldsymbol{e}_{p,2}}{\Upsilon_1}\right) - \boldsymbol{e}_{a,2}^T \hat{\tilde{\mu}}_a \tanh\left(\frac{\boldsymbol{e}_{a,2}}{\Upsilon_2}\right) \\ & + \boldsymbol{e}_{p,2}^T \mu_p (\boldsymbol{Z}_p) + \boldsymbol{e}_{a,2}^T \mu_a (\boldsymbol{Z}_a) \end{aligned} \tag{52}$$

Based on(52), a Lyapunov function can be established as follows:

$$\begin{aligned} V_2 = V_f + V_1 + \frac{1}{2} \left(\tilde{\boldsymbol{W}}_p^T \boldsymbol{k}_{w1}^{-1} \tilde{\boldsymbol{W}}_p \right) + \frac{1}{2} \left(\tilde{\boldsymbol{W}}_a^T \boldsymbol{k}_{w3}^{-1} \tilde{\boldsymbol{W}}_a \right) \\ + \frac{1}{2} \left(\tilde{\tilde{\boldsymbol{\mu}}}_p^T \boldsymbol{k}_{\mu 1}^{-1} \tilde{\tilde{\boldsymbol{\mu}}}_p \right) + \frac{1}{2} \left(\tilde{\tilde{\boldsymbol{\mu}}}_a^T \boldsymbol{k}_{\mu 2}^{-1} \tilde{\tilde{\boldsymbol{\mu}}}_a \right) \end{aligned} \tag{53}$$

Differentiating (53) with respect to time yields

$$\begin{aligned} \dot{V}_2 = \dot{V}_f + \dot{V}_1 + \boldsymbol{k}_{w1}^{-1} \left(\tilde{W}_p^T \dot{\tilde{W}}_p \right) + \boldsymbol{k}_{w3}^{-1} \left(\tilde{W}_a^T \dot{\tilde{W}}_a \right) \\ + \boldsymbol{k}_{\mu 1}^{-1} \left(\tilde{\tilde{\mu}}_p^T \dot{\tilde{\tilde{\mu}}}_p \right) + \boldsymbol{k}_{\mu 2}^{-1} \left(\tilde{\tilde{\mu}}_a^T \dot{\tilde{\tilde{\mu}}}_a \right) \end{aligned} \tag{54}$$

By recalling Lemma 2, and according to Young's inequality, we can obtain that the following inequation holds:

$$\begin{aligned} \tilde{\boldsymbol{W}}_p^T \hat{\boldsymbol{W}}_p &\leq \frac{1}{2} \left(\boldsymbol{W}_p^* \right)^T \boldsymbol{W}_p^* - \frac{1}{2} \tilde{\boldsymbol{W}}_p^T \tilde{\boldsymbol{W}}_p \\ \tilde{\boldsymbol{W}}_a^T \hat{\boldsymbol{W}}_a &\leq \frac{1}{2} \left(\boldsymbol{W}_a^* \right)^T \boldsymbol{W}_a^* - \frac{1}{2} \tilde{\boldsymbol{W}}_a^T \tilde{\boldsymbol{W}}_a \end{aligned} \tag{55}$$

Based on Lemma 3, the following equation holds:

$$\begin{aligned} \tilde{\tilde{\boldsymbol{\mu}}}_p^T \hat{\tilde{\boldsymbol{\mu}}}_p^{q_5} &\leq \frac{1}{1+q_5} (2 \bar{\boldsymbol{\mu}}_p^{1+q_5} - \tilde{\boldsymbol{\mu}}_p^{1+q_5}) \\ \tilde{\tilde{\boldsymbol{\mu}}}_p^T \hat{\tilde{\boldsymbol{\mu}}}_p^{q_6} &\leq \frac{1}{1+q_6} (2 \bar{\boldsymbol{\mu}}_p^{1+q_6} - \tilde{\boldsymbol{\mu}}_p^{1+q_6}) \\ \tilde{\tilde{\boldsymbol{\mu}}}_a^T \hat{\tilde{\boldsymbol{\mu}}}_a^{q_5} &\leq \frac{1}{1+q_5} (2 \bar{\boldsymbol{\mu}}_a^{1+q_5} - \tilde{\boldsymbol{\mu}}_a^{1+q_5}) \\ \tilde{\tilde{\boldsymbol{\mu}}}_a^T \hat{\tilde{\boldsymbol{\mu}}}_a^{q_6} &\leq \frac{1}{1+q_6} (2 \bar{\boldsymbol{\mu}}_a^{1+q_6} - \tilde{\boldsymbol{\mu}}_a^{1+q_6}) \end{aligned} \tag{56}$$

Furthermore, substituting Eqs. (48) and (49) into Eq. (56), can be simplified as

$$\begin{aligned} \dot{V}_2 \leq & -k_f V_f - \boldsymbol{k}_{p,2} \boldsymbol{\varepsilon}_p^2 - \boldsymbol{k}_{a,2} \boldsymbol{\varepsilon}_a^2 - \boldsymbol{k}_{p,4} \boldsymbol{e}_{p,2}^2 - \boldsymbol{k}_{a,4} \boldsymbol{e}_{a,2}^2 \\ & - \frac{k_{p,6}}{1+q_6} \tilde{\tilde{\boldsymbol{\mu}}}_p^2 - \frac{k_{a,6}}{1+q_6} \tilde{\tilde{\boldsymbol{\mu}}}_a^2 - \frac{k_{w2}}{2} \tilde{\boldsymbol{W}}_p^T \tilde{\boldsymbol{W}}_p \\ & - \frac{k_{w4}}{2} \tilde{\boldsymbol{W}}_a^T \tilde{\boldsymbol{W}}_a + \Omega \end{aligned} \tag{57}$$

where

$$\begin{aligned} \Omega = & \frac{2p_{p,1}}{1+q_m} \left(\eta_p^2\right)^{\frac{1+q_m}{2}} + \frac{2p_{p,2}}{1+q_n} \left(\eta_p^2\right)^{\frac{1+q_n}{2}} + \frac{2p_{a,1}}{1+q_m} \left(\eta_a^2\right)^{\frac{1+q_m}{2}} \\ & + \frac{2p_{a,2}}{1+q_n} \left(\eta_a^2\right)^{\frac{1+q_n}{2}} + \frac{2k_{p,5}}{1+q_5} \left(\bar{\boldsymbol{\mu}}_p^2\right)^{\frac{1+q_5}{2}} + \frac{2k_{p,6}}{1+q_6} \left(\bar{\boldsymbol{\mu}}_p^2\right)^{\frac{1+q_6}{2}} \\ & + \frac{2k_{a,5}}{1+q_5} \left(\bar{\boldsymbol{\mu}}_a^2\right)^{\frac{1+q_5}{2}} + \frac{2k_{a,6}}{1+q_6} \left(\bar{\boldsymbol{\mu}}_a^2\right)^{\frac{1+q_6}{2}} + \frac{k_{w2}}{2} \left(\mathbf{W}_p^*\right)^T \mathbf{W}_p^* \\ & + \frac{k_{w4}}{2} \left(\boldsymbol{W}_a^*\right)^T \boldsymbol{W}_a^* + k_1 \Upsilon_1 \left|\bar{\boldsymbol{\mu}}_p\right| + k_2 \Upsilon_2 \left|\bar{\boldsymbol{\mu}}_a\right| + k \left(\sigma_p + \sigma_a\right) \end{aligned}$$

is a nonnegative constant.

Then, (57) can be further formulated as follows:

$$\dot{V}_2 \leq -k_{v2} V_2 + \Omega \tag{58}$$

where

$$\begin{aligned} k_{v2} = \min \Bigg\{ & k_f, \boldsymbol{k}_{p,2}, \boldsymbol{k}_{a,2}, \boldsymbol{k}_{p,4}, \boldsymbol{k}_{a,4}, \frac{k_{p,5}}{1+q_5}, \frac{k_{p,6}}{1+q_6}, \\ & \frac{k_{a,5}}{1+q_5}, \frac{k_{a,6}}{1+q_6}, \frac{k_{w2}}{2}, \frac{k_{w4}}{2} \Bigg\} > 0. \end{aligned}$$

The inequality (58) can be further computed as

$$0 \leq V_2(t) \leq \frac{\Omega}{k_{v2}} \left(1 - \exp\left(-k_{v2} t\right)\right) + V_2(0) \exp\left(-k_{v2} t\right) \tag{59}$$

Thus, there exists an upper bound on the error signals $\xi_p, \xi_a, \boldsymbol{\varepsilon}_p, \boldsymbol{\varepsilon}_a, \boldsymbol{e}_{p,2}, \boldsymbol{e}_{a,2}, \tilde{\bar{\boldsymbol{\mu}}}_p, \tilde{\bar{\boldsymbol{\mu}}}_a, \tilde{\boldsymbol{W}}_p, \tilde{\boldsymbol{W}}_a$ of the closed-loop system for quadrotor dynamics, which are bounded by the following inequality:

$$\begin{aligned} \left\|\xi_p\right\| &\le \sqrt{2\Omega/k_{v2}} \quad \|\xi_a\| \le \sqrt{2\Omega/k_{v2}} \\ \left\|\boldsymbol{\varepsilon}_p\right\| &\le \sqrt{2\Omega/k_{v2}} \quad \|\boldsymbol{\varepsilon}_a\| \le \sqrt{2\Omega/k_{v2}} \\ \left\|\boldsymbol{e}_{p,2}\right\| &\le \sqrt{2\Omega/k_{v2}} \quad \left\|\boldsymbol{e}_{a,2}\right\| \le \sqrt{2\Omega/k_{v2}} \\ \left\|\tilde{\bar{\boldsymbol{\mu}}}_p\right\| &\le \sqrt{2\Omega/k_{v2}} \quad \left\|\tilde{\bar{\boldsymbol{\mu}}}_a\right\| \le \sqrt{2\Omega/k_{v2}} \\ \left\|\tilde{\boldsymbol{W}}_p\right\| &\le \sqrt{2\Omega/k_{v2}} \quad \left\|\tilde{\boldsymbol{W}}_a\right\| \le \sqrt{2\Omega/k_{v2}} \end{aligned} \tag{60}$$

The closed-loop tracking error signal mentioned earlier can potentially converge to a small residual set, which can be minimized by appropriately adjusting the controller parameters. Furthermore, by recalling Theorem 1 and coupling with $\left\|\boldsymbol{\varepsilon}_p\right\| \le \sqrt{2\Omega/k_{v2}}, \|\boldsymbol{\varepsilon}_a\| \le \sqrt{2\Omega/k_{v2}}$, which implies that the tracking error state can be limited to satisfy (20). Further analysis reveals the existence of a nonnegative constant σ_w that satisfies $\tilde{W}_i^T \tilde{W}_i \le \sigma_w$.

To demonstrate that the tracking error in the closed-loop control system converges to near zero in a fixed time. If any real constants $x > 0$, the following inequalities hold:

$$x^{\frac{b+1}{2}} - x \le \left(\frac{b+1}{2}\right)^{\frac{b+1}{1-b}} - \left(\frac{b+1}{2}\right)^{\frac{2}{1-b}} = \prod \tag{61}$$

Subsequently, to further demonstrate that the closed-loop system achieves fixed-time stability, Eq. (57) can be expressed as

$$\dot{V}_2 \le -k_1 V_2^q - k_2 V_2^p + \Lambda \tag{62}$$

where

$$\begin{aligned} q &= \frac{1+q_m}{2} = \frac{1+q_1}{2} = \frac{1+q_3}{2} = \frac{1+q_5}{2}; \\ p &= \frac{1+q_n}{2} = \frac{1+q_2}{2} = \frac{1+q_4}{2} = \frac{1+q_6}{2}; \\ k_1 &= \min\left\{\boldsymbol{k}_{p,1}, \boldsymbol{k}_{a,1}, \boldsymbol{k}_{p,3}, \boldsymbol{k}_{a,3}, \frac{1}{T_p}, \frac{1}{T_a}, \right. \\ &\quad \left. \frac{p_{p,1}}{1+q_m}, \frac{p_{a,1}}{1+q_m}, \frac{k_{p,5}}{1+q_5}, \frac{k_{a,5}}{1+q_5} \frac{k_{w2}}{2}, \frac{k_{w4}}{2}\right\} \\ k_2 &= \min\left\{\boldsymbol{k}_{p,2}, \boldsymbol{k}_{a,2}, \boldsymbol{k}_{p,4}, \boldsymbol{k}_{a,4}, \frac{1}{T_p}, \frac{1}{T_a}, \right. \\ &\quad \left. \frac{p_{p,2}}{1+q_n}, \frac{p_{a,2}}{1+q_n}, \frac{k_{p,6}}{1+q_6}, \frac{k_{a,6}}{1+q_6}, \frac{k_{w2}}{2}, \frac{k_{w4}}{2}\right\} \\ \Lambda &= \frac{2p_{p,1}}{1+q_m}\left(\eta_p^2\right)^{\frac{1+q_m}{2}} + \frac{2p_{p,2}}{1+q_n}\left(\eta_p^2\right)^{\frac{1+q_n}{2}} + \frac{2p_{a,1}}{1+q_m}\left(\eta_a^2\right)^{\frac{1+q_m}{2}} \\ &\quad + \frac{2p_{a,2}}{1+q_n}\left(\eta_a^2\right)^{\frac{1+q_n}{2}} + \frac{2k_{p,5}}{1+q_5}\left(\bar{\mu}_p^2\right)^{\frac{1+q_5}{2}} + \frac{2k_{p,6}}{1+q_6}\left(\bar{\mu}_p^2\right)^{\frac{1+q_6}{2}} \\ &\quad + \frac{2k_{a,5}}{1+q_5}\left(\bar{\mu}_a^2\right)^{\frac{1+q_5}{2}} + \frac{2k_{a,6}}{1+q_6}\left(\bar{\mu}_a^2\right)^{\frac{1+q_6}{2}} + \frac{k_{w2}}{2}\left(\mathbf{W}_p^*\right)^T \mathbf{W}_p^* \\ &\quad + \frac{k_{w4}}{2}\left(\boldsymbol{W}_a^*\right)^T \boldsymbol{W}_a^* + k_1\Upsilon_1\left|\bar{\mu}_p\right| + k_2\Upsilon_2\left|\bar{\mu}_a\right| + k\left(\sigma_p + \sigma_a\right) \\ &\quad + 2\Pi + \sigma_{w1} + \sigma_{w2} \end{aligned}$$

Based on Lemma 1, all the error signals will converge to the region set

$$x \in \left\{V_2 \le \min\left\{\left(\frac{\Lambda}{k_1\left(1-\varpi\right)}\right)^{\frac{1}{q}}, \left(\frac{\Lambda}{k_2\left(1-\varpi\right)}\right)^{\frac{1}{p}}\right\}\right\}$$

near zero in a fixed time

$$T_g \le \frac{1}{k_1\varpi\left(1-q\right)} + \frac{1}{k_2\varpi\left(p-1\right)} \tag{63}$$

Based on the stability analysis above, the proposed control strategy can effectively address the tracking control challenges caused by model parameter uncertainties, mutational external disturbances, and input saturation. In combination with Theorem 1 and (60), the trajectory tracking error can be constrained to satisfy (20) and guarantee that the tracking error of the closed-loop system converges to near zero within a fixed time. The whole closed-loop system achieves fixed-time stability.

The proof of Theorem 2 ends

Remark 5: Because the proposed strategy involves many control parameters, it is quite difficult to obtain an optimal solution. To ensure that the error signal can converge to within the prescribed performance envelope in a fixed time, we can satisfy the determination of the gain parameter of the controller by the trial-and-error method.

IV. SIMULATIONS

In this section, the superiority and efficiency of the proposed method are evaluated by simulations and comparative experiments. Time-varying trajectory tracking and external disturbance scenarios are considered, and the algorithm is implemented in the MATLAB/SIMULINK platform with a fixed-step solver and a sampling time of 0.001 s for all control algorithms.

By referring to [38], the model parameters of quadrotors are chosen as follows: $m = 2\,\text{kg}$, $l = 0.2\text{m}$, $\boldsymbol{J} = diag\{1.25, 1.25, 2.5\}\,\text{N}\cdot\text{s}^2/\text{rad}$, $g = 9.8\,\text{m/s}^2 c = 1.14 \cdot 10^{-7}\text{N}\cdot$, $\text{s}^2/\text{rad}^2 b = 2.98 \cdot 10^{-6}\text{N}\cdot\text{s}^2/\text{rad}^2$, $\boldsymbol{K}_p = diag\{1.2, 1.2, 1.2\} \cdot 10^{-2}\text{N}\cdot\text{s/rad}$, and $\boldsymbol{K}_a = diag\{1.2, 1.2, 1.2\} \cdot 10^{-2}\text{N}\cdot\text{s/rad}$, and the associated parameters of the controllers are listed in Table 1.

The initial number of neurons in the SSNN is selected as $N = 21$, the initial conditions of the adaptive law are selected as $\hat{W}_p = \hat{W}_a = [0, 0, 0]^T$, and the center of the Gaussian functions is uniformly distributed in $[-5, 5]$ with a width of 0.5. The splitting threshold G_{th} and the delete threshold P_{th} are designed as 0.8 and 0.3, respectively.

To verify that the proposed control algorithm can achieve fixed-time trajectory tracking under a mutational external disturbance, the trajectory reference signal and mutational external disturbance are considered as follows:

The reference trajectory is given as follows:

$$\mathbf{p}_d = \begin{cases} x_d = 8\cos\left(0.3t\right) \\ y_d = 4\sin\left(0.6t\right) \\ z_d = 0.5t \end{cases} \tag{64}$$

TABLE 1. Design parameters of the proposed algorithm.

Module	Value
APPC	$\rho_0^x=\rho_0^y=\rho_0^z=4$; $\rho_0^\phi=\rho_0^\theta=\rho_0^\psi=4$; $\rho_\infty^x=\rho_\infty^y=\rho_\infty^z=0.1$;
	$\rho_\infty^\phi=\rho_\infty^\theta=\rho_\infty^\psi=0.1$; $\gamma_x=\gamma_y=\gamma_z=0.2$; $\gamma_\phi=\gamma_\theta=\gamma_\psi=0.2$;
	$k_{1,x}=k_{1,y}=k_{1,z}=0.9$; $k_{1,\phi}=k_{1,\theta}=k_{1,\psi}=0.9$;
	$k_{2,x}=k_{2,y}=k_{2,z}=1.5$; $k_{2,\phi}=k_{2,\theta}=k_{2,\psi}=1.5$
	$k_{s,1}=2.5$; $k_{s,2}=0.01$;
DSC	$T=\left[0.1,0.1,0.1,0.02,0.02,0.02\right]^T$;
	$p_{x,1}=p_{y,1}=p_{z,1}=0.05$; $p_{\phi,1}=p_{\theta,1}=p_{\psi,1}=0.05$;
	$p_{x,2}=p_{y,2}=p_{z,2}=0.05$; $p_{\phi,2}=p_{\theta,2}=p_{\psi,2}=0.05$
Controller	$\boldsymbol{k}_{p,1}=diag\left\{0.15,0.15,0.15\right\}$; $\boldsymbol{k}_{p,2}=diag\left\{0.15,0.15,0.15\right\}$;
	$\boldsymbol{k}_{p,3}=diag\left\{1.25,1.25,1.25\right\}$; $\boldsymbol{k}_{p,4}=diag\left\{1.25,1.25,1.25\right\}$;
	$\boldsymbol{k}_{a,1}=diag\left\{2.8,2.8,2.8\right\}$; $\boldsymbol{k}_{a,2}=diag\left\{2.8,2.8,2.8\right\}$;
	$\boldsymbol{k}_{a,3}=diag\left\{20,20,20\right\}$; $\boldsymbol{k}_{a,4}=diag\left\{20,20,20\right\}$;
SSNN	$k_{w1}=300$; $k_{w2}=1$; $k_{w3}=50$; $k_{w4}=1$;
	$k_{\mu1}=10$; $k_{\mu2}=10$; $\Upsilon_1=0.8$; $\Upsilon_2=0.8$;
	$\boldsymbol{k}_{p,5}=diag\left\{1.4,1.4,1.4\right\}$; $\boldsymbol{k}_{p,6}=diag\left\{1.2,1.2,1.2\right\}$;
	$\boldsymbol{k}_{a,5}=diag\left\{1.2,1.2,1.2\right\}$; $\boldsymbol{k}_{a,6}=diag\left\{1.4,1.4,1.4\right\}$;
Fixed-time parameters	$q_m=q_1=q_3=q_5=0.6$; $q_n=q_2=q_4=q_6=3$;

The mutational external disturbances are given as

$$\mathbf{D}_p=\left[d_x,d_y,d_z\right]^T=\begin{cases}[1.2\sin(0.2t)\cos(0.2t),\\ 1.6\cos(0.1t)\sin(0.3t),\\ 1.3\sin(0.4t)\cos(0.2t)]^T, & t<30\\ [6\sin(0.4t)\cos(0.4t),\\ 6\cos(0.2t)\sin(0.4t),\\ 6\sin(0.4t)\cos(0.4t)]^T, & t\geq 30\end{cases}$$

$$\mathbf{D}_a=\left[d_\phi,d_\theta,d_\psi\right]^T=\begin{cases}[0.3\sin(0.2t)\cos(0.2t),\\ 0.2\cos(0.2t)\sin(0.1t),\\ 0.5\sin(0.2t)\cos(0.3t)]^T, & t<30\\ [2\sin(0.4t)\cos(0.4t),\\ 2\cos(0.2t)\sin(0.4t),\\ 2\sin(0.4t)\cos(0.3t)]^T, & t\geq 30\end{cases} \tag{65}$$

The initial position and angle states are set as $\mathbf{p}(0)=[7,1,0]^T$ m and $\mathbf{\Theta}(0)=[0,0,-\pi/4]^T$, respectively, and the desired yaw angle is chosen as $\Theta_\psi^d=0$ rad.

Case 1: Verify the effectiveness of the proposed control method

The simulation results are presented in Figs. 5-11. Specifically, Fig. 5 illustrates the three-dimensional trajectory tracking results, indicating that the quadrotor is capable of tracking the desired path with high speed and accuracy. Fig. 6 indicates the trajectory control error under the APPF,

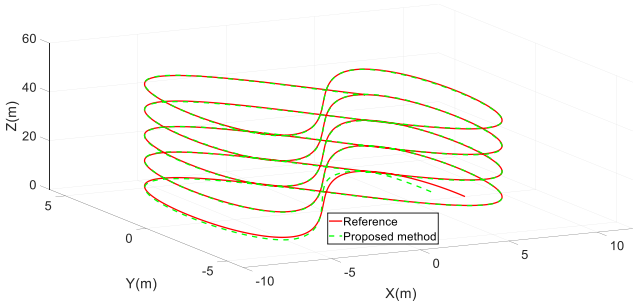

FIGURE 5. 3D trajectory tracking.

and the mutation external disturbance occurs in the 30th second. By employing the adjustable boundary and SSNN, the singularity problem caused by the mutation disturbance is avoided, and the estimated disturbance can be adjusted online rapidly and fed back to the controller in time to eliminate the influence of the external disturbance. Fig. 7 depicts the response curves of position and attitude tracking, which demonstrate that the proposed controller exhibits strong robustness against mutation external disturbances and that both the trajectory and attitude states can ultimately achieve uniformly bounded results. From Fig. 8, we find that a mutation disturbance occurs at 30 seconds, and the external disturbance is compensated according to the estimated value of the SSNN feedback. Fig. 9 shows that the filtering error converges quickly to a small value even when a mutation

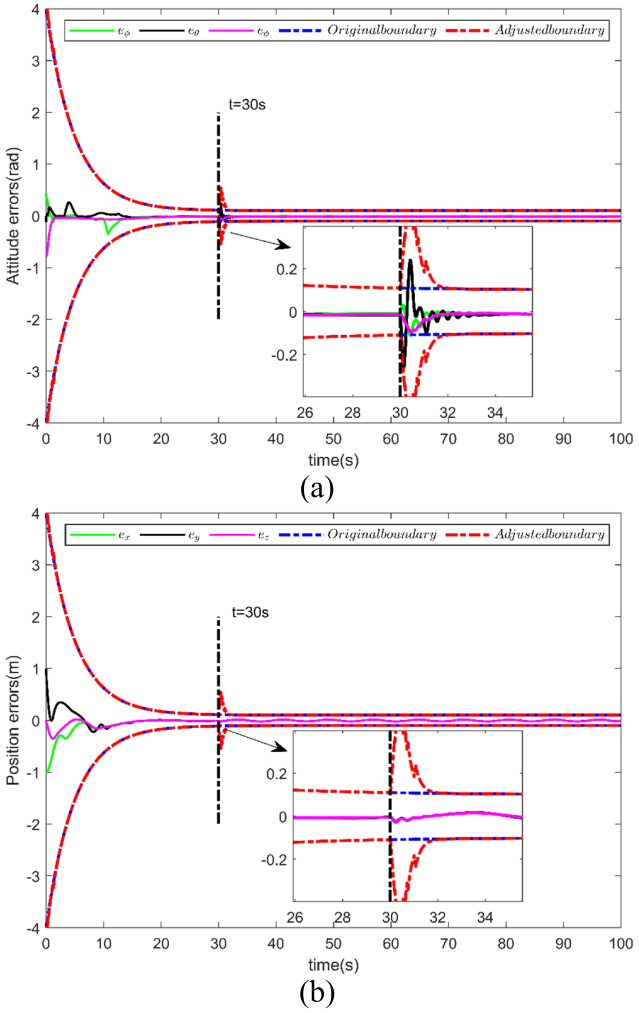

FIGURE 6. Trajectory tracking error constraints within a mutational external disturbance (a)attitude system, (b)position system.

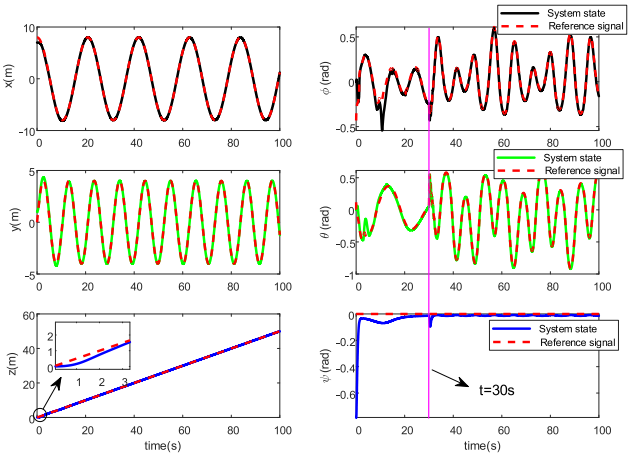

FIGURE 7. Six-directional trajectory tracking.

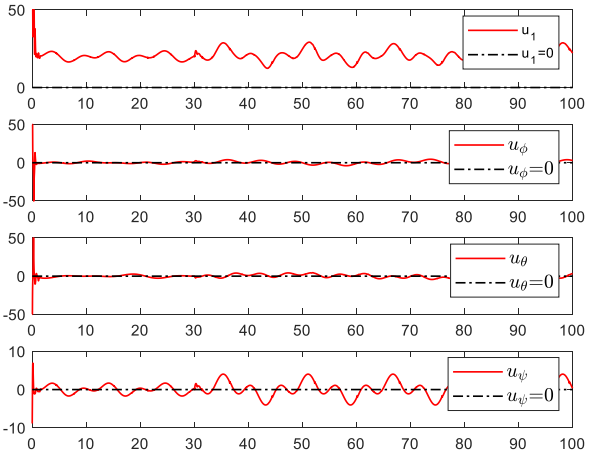

FIGURE 8. Control inputs.

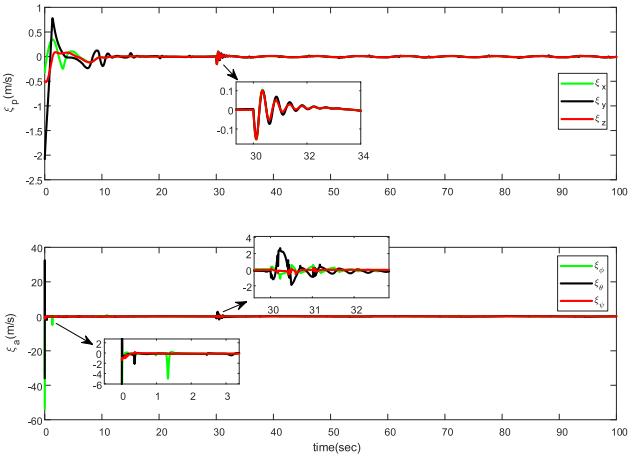

FIGURE 9. Filtering errors.

disturbance is encountered. Fig. 10 illustrates the adaptive law of the upper limit of the derivative of the fixed-time command filter used to estimate the virtual control input over time, which facilitates realtime updating of the filter parameters and enables the filter to adapt to system changes. The change in the number of neurons in the SSNN is provided in Fig. 11, which indicates that the initial number of neurons is 21, and the final number of neurons remains stable at 18 and 15 even though the mutation disturbance occurs at the 30th second. Fig. 12 illustrates the weight estimates of the SSNN, which are still bounded even if the mutation disturbance appears after 30 seconds. The results presented in Figs. 11-12 show that the proposed SSNN is capable of adjusting the number of neurons in real time, reducing the computational burden while remaining stable and bounded when dealing with mutational disturbances. The adaptability of the SSNN ensures that it retains only effective neurons while eliminating ineffective neurons, leading to better approximation performance.

Case 2: Comparative study against finite-time controller [23] Subsequently, a comparative study is performed by comparison with the finite-time control method under the same environmental conditions to prove the superiority of the proposed control strategy.

TABLE 2. Designed parameters of the finite-time controller [22].

Parameters	Value	Parameters	Value
$\lambda_{1,p}$	4.00	$k_{t,1}$	0.10
$\lambda_{2,p}$	3.00	$k_{t,2}$	20.00
$\lambda_{3,p}$	3.00	$k_{t,3}$	0.20
$\lambda_{1,a}$	1.00	$k_{t,4}$	10.00
$\lambda_{2,a}$	3.00	α_p	1.50
$\lambda_{3,a}$	3.00	β_p	0.50
L_1	0.002	α_a	1.50
L_2	0.0002	β_a	0.50

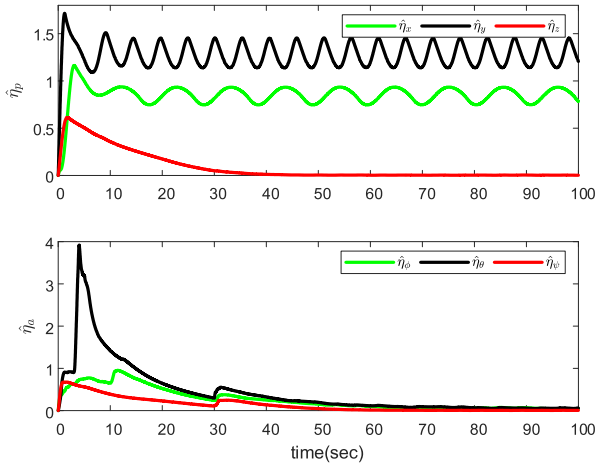

FIGURE 10. Adaptive laws of the filter.

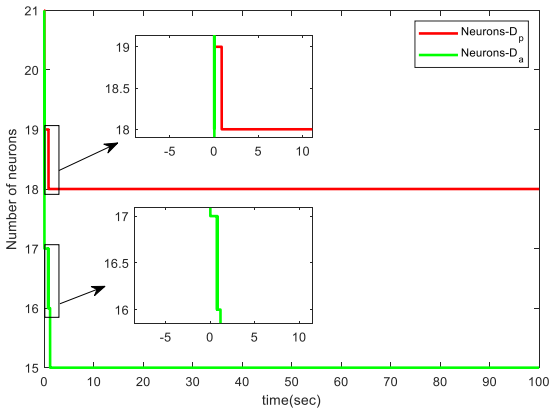

FIGURE 11. The number of neurons.

The finite-time disturbance observer for the position subsystem is proposed as follows:

$$\begin{aligned}
\dot{z}_{1,i} &= v_{1,i} + \alpha_i v_i + \left(sat\left(\tau_f\right)\Xi_{(i)} - g\mathbf{E}\right)\\
w_{1,i} &= -\lambda_{1,p}L_1^{1/3}\left|z_{1,p} - v_i\right|^{(2/3)} sign\left(z_{1,p} - v_i\right) + z_{2,i}\\
\dot{z}_{2,i} &= w_{2,i}
\end{aligned}$$

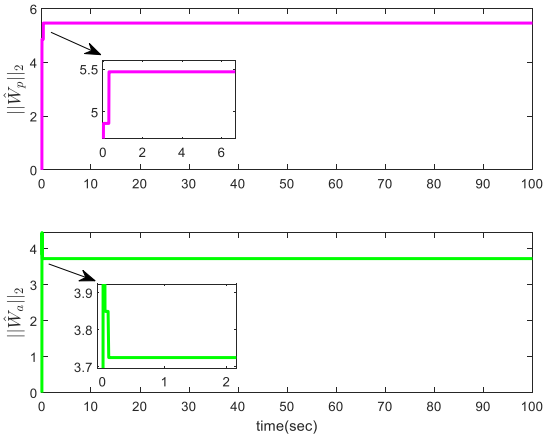

FIGURE 12. The 2-norm of the SSNN weight estimate $\left\|\hat{W}_p\right\|$ and $\left\|\hat{W}_a\right\|$.

$$\begin{aligned}
v_{2,i} &= -\lambda_{2,p}L_1^{1/3}\left|z_{2,p} - w_{1,i}\right|^{(1/2)} sign\left(z_{2,p} - w_{1,i}\right) + z_{3,i}\\
\dot{z}_{3,i} &= -\lambda_{3,p}L_1^{1/3}\left|z_{3,p} - w_{2,i}\right| sign\left(z_{3,p} - w_{2,i}\right) i = (x, y, z)
\end{aligned} \tag{66}$$

The finite-time disturbance observer for the attitude subsystem is given as:

$$\begin{aligned}
\dot{z}_{1,j} &= v_{1,j} + \alpha_j\omega_j - J_j^{-1}sat\left(\tau_j\right)\\
w_{1,j} &= -\lambda_{1,a}L_2^{1/3}\left|z_{1,a} - \omega_j\right|^{(2/3)} sign\left(z_{1,a} - \omega_j\right) + z_{2,j}\\
\dot{z}_{2,j} &= w_{2,j}\\
v_{2,j} &= -\lambda_{2,a}L_2^{1/3}\left|z_{2,a} - w_{1,j}\right|^{(1/2)} sign\left(z_{2,a} - w_{1,j}\right) + z_{3,j}\\
\dot{z}_{3,j} &= -\lambda_{3,a}L_2^{1/3}\left|z_{3,a} - w_{2,j}\right| sign\left(z_{3,a} - w_{2,j}\right) j = (\phi, \theta, \psi)
\end{aligned} \tag{67}$$

The finite-time control strategy for the trajectory loop is designed as follows:

$$\begin{aligned}
s_{p,i} &= e_{1,i} + \beta_p\left|\dot{e}_{1,i}\right|^{\alpha_p} sign\left(\dot{e}_{1,i}\right)\\
\tau_f &= -\frac{m}{\cos\phi\cos\theta}\left[\frac{1}{\alpha_z\beta_z}\left|\dot{e}_{1,z}\right|^{2-\alpha_p} + k_{t,1}s_{p,z}\right.\\
&\quad \left. + k_{t,2}\left|s_{p,z}\right|^{\alpha_p} sign\left(\dot{e}_{1,z}\right)\right]
\end{aligned} \tag{68}$$

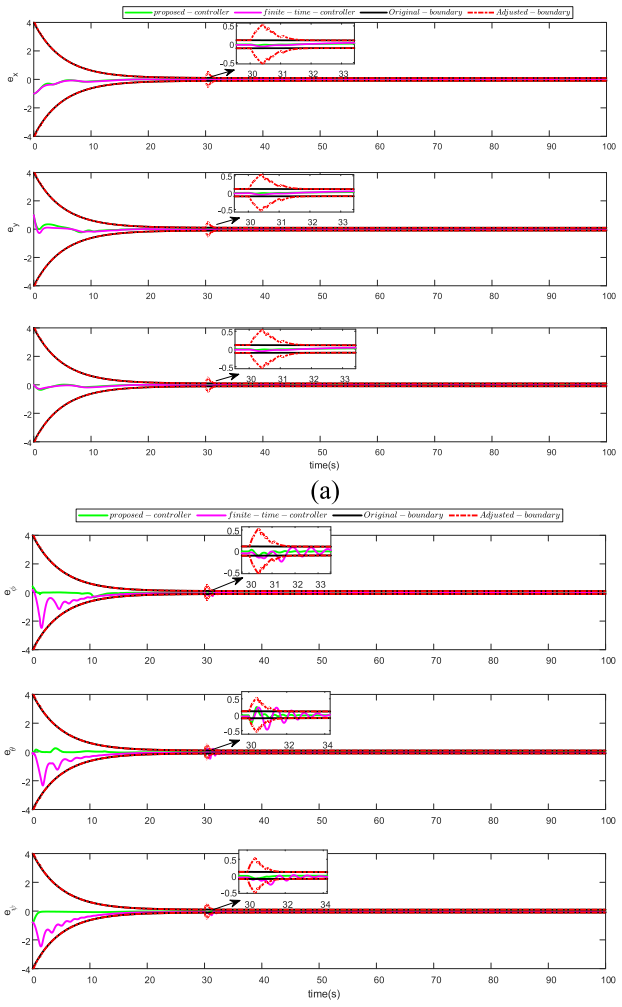

FIGURE 13. Trajectory tracking error constraiTrajectory tracking error constraints compared with a finite-time controller [23](a) position subsystem, (b) attitude subsystem.

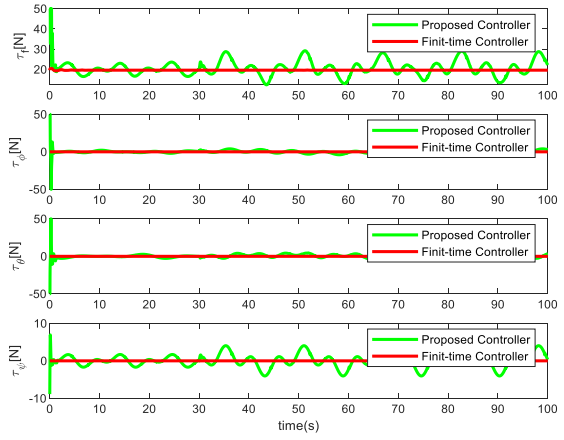

FIGURE 14. Comparison of two control strategy inputs.

For the attitude loop:

$$s_{a,j} = e_{a,1} + \beta_a \left|\dot{e}_{a,1}\right|^{\alpha_a} sign\left(\dot{e}_{a,1}\right)$$

$$\tau_j = -\frac{1}{b_j}\left[-\frac{1}{\alpha_j J_j^{-1}}\left|\dot{e}_{a,1}\right|^{2-\alpha_a} + k_{t,3}s_{a,1} + k_{t,4}\left|s_{a,1}\right|^{\alpha_a} sign\left(s_{a,1}\right) + \alpha_j\omega_j + \ddot{\Theta}_j^d + z_{2,j}\right] \quad (69)$$

where $s_{p,i}$ and $s_{a,j}$ denote the sliding surface, $\alpha_i = -K_i/m$ and $\alpha_j = -J_i^{-1}K_j$. The controller gains are set in Table 2.

Fig. 13 illustrates the trajectory tracking performance of the proposed controller and finite-time controller with the same environmental conditions. The proposed controller exhibits faster convergence within the first 30 seconds, with a quicker response and effective constraint of the tracking error within the boundaries. Furthermore, even in the presence of mutation disturbances after 30 seconds, the proposed controller maintains superior performance compared to the finite-time controller. Fig. 14 demonstrates that the proposed controller achieves stable convergence of the quadrotor system with a faster response compared to finite-time control, even in the presence of mutation disturbances, and requires lower resource consumption. Thus, the abovementioned analysis demonstrates the effectiveness and usefulness of the proposed controller in handling lump disturbances, including unknown external disturbances and uncertain nonlinear functions, while adjusting the number of neurons in real time to reduce the computational burden and improve the approximation accuracy for quadrotors with limited onboard resources.

V. CONCLUSION

In this article, an adjustable prescribed performance method is proposed for quadrotor UAVs dealing with mutation disturbances and actuator saturation. This method enables adaptive adjustment of predetermined performance boundaries without compromising convergence speed. It also addresses the potential singularity problem arising from tracking error peaks. By utilizing a self-structuring neural network and compensating for lump disturbances, the proposed control method achieves high-accuracy trajectory tracking for practical quadrotors with limited onboard resources. This makes the proposed method practical and feasible for quadrotors operating in real-world environments. Further work will promote the existing algorithms, which will be considered for practical applications such as actuator failure and obstacle avoidance, and to achieve a networked quadrotor distributed formation coordination control design.

REFERENCES

[1] X. Liang, H. Yu, Z. Zhang, H. Liu, Y. Fang, and J. Han, "Unmanned aerial transportation system with flexible connection between the quadrotor and the payload: Modeling, controller design, and experimental validation," *IEEE Trans. Ind. Electron.*, vol. 70, no. 2, pp. 1870–1882, Feb. 2023.

[2] Y. Cai, K. Guan, E. Nafziger, G. Chowdhary, B. Peng, Z. Jin, S. Wang, and S. Wang, "Detecting in-season crop nitrogen stress of corn for field trials using UAV- and CubeSat-based multispectral sensing," *IEEE J. Sel. Topics Appl. Earth Observ. Remote Sens.*, vol. 12, no. 12, pp. 5153–5166, Dec. 2019.

[3] J. Wang, C. Bi, D. Wang, Q. Kuang, and C. Wang, "Finite-time distributed event-triggered formation control for quadrotor UAVs with experimentation," *ISA Trans.*, vol. 126, pp. 585–596, Jul. 2022.
[4] R. Wang and J. Liu, "Trajectory tracking control of a 6-DOF quadrotor UAV with input saturation via backstepping," *J. Franklin Inst.*, vol. 355, no. 7, pp. 3288–3309, May 2018.
[5] J. Tan and S. Guo, "Backstepping control with fixed-time prescribed performance for fixed wing UAV under model uncertainties and external disturbances," *Int. J. Control*, vol. 95, no. 4, pp. 934–951, Apr. 2022.
[6] H. Lee, S. Yoon, and S. Han, "Robust attitude control scheme for constantly spinning small-sized quadrotor in the presence of imbalance characteristics," *IEEE Trans. Aerosp. Electron. Syst.*, vol. 58, no. 2, pp. 1405–1415, Apr. 2022.
[7] J. R. S. Benevides, M. A. D. Paiva, P. V. G. Simplício, R. S. Inoue, and M. H. Terra, "Disturbance observer-based robust control of a quadrotor subject to parametric uncertainties and wind disturbance," *IEEE Access*, vol. 10, pp. 7554–7565, 2022.
[8] X.-Z. Jin, W.-W. Che, Z.-G. Wu, and C. Deng, "Robust adaptive general formation control of a class of networked quadrotor aircraft," *IEEE Trans. Syst., Man, Cybern., Syst.*, vol. 52, no. 12, pp. 7714–7726, Dec. 2022.
[9] S. Wang, A. Polyakov, and G. Zheng, "Quadrotor stabilization under time and space constraints using implicit PID controller," *J. Franklin Inst.*, vol. 359, no. 4, pp. 1505–1530, Mar. 2022.
[10] X. Shao, J. Liu, and H. Wang, "Robust back-stepping output feedback trajectory tracking for quadrotors via extended state observer and sigmoid tracking differentiator," *Mech. Syst. Signal Process.*, vol. 104, pp. 631–647, May 2018.
[11] L. Chen, Z. Liu, Q. Dang, W. Zhao, and G. Wang, "Robust trajectory tracking control for a quadrotor using recursive sliding mode control and nonlinear extended state observer," *Aerosp. Sci. Technol.*, vol. 128, Sep. 2022, Art. no. 107749.
[12] M. Islam, M. Okasha, and E. Sulaeman, "A model predictive control (MPC) approach on unit quaternion orientation based quadrotor for trajectory tracking," *Int. J. Control, Autom. Syst.*, vol. 17, no. 11, pp. 2819–2832, Nov. 2019.
[13] H. Razmi and S. Afshinfar, "Neural network-based adaptive sliding mode control design for position and attitude control of a quadrotor UAV," *Aerosp. Sci. Technol.*, vol. 91, pp. 12–27, Aug. 2019.
[14] A. Polyakov, "Nonlinear feedback design for fixed-time stabilization of linear control systems," *IEEE Trans. Autom. Control*, vol. 57, no. 8, pp. 2106–2110, Aug. 2012.
[15] K. Liu, R. Wang, S. Zheng, S. Dong, and G. Sun, "Fixed-time disturbance observer-based robust fault-tolerant tracking control for uncertain quadrotor UAV subject to input delay," *Nonlinear Dyn.*, vol. 107, no. 3, pp. 2363–2390, Feb. 2022.
[16] B. Li, W. Gong, Y. Yang, B. Xiao, and D. Ran, "Appointed fixed time observer-based sliding mode control for a quadrotor UAV under external disturbances," *IEEE Trans. Aerosp. Electron. Syst.*, vol. 58, no. 1, pp. 290–303, Feb. 2022.
[17] F. Wang, Z. Ma, H. Gao, C. Zhou, and C. Hua, "Disturbance observer-based nonsingular fast terminal sliding mode fault tolerant control of a quadrotor UAV with external disturbances and actuator faults," *Int. J. Control, Autom. Syst.*, vol. 20, no. 4, pp. 1122–1130, Apr. 2022.
[18] G. Cui, W. Yang, J. Yu, Z. Li, and C. Tao, "Fixed-time prescribed performance adaptive trajectory tracking control for a QUAV," *IEEE Trans. Circuits Syst. II, Exp. Briefs*, vol. 69, no. 2, pp. 494–498, Feb. 2022.
[19] Y. Zhang, G. Wu, X. Yang, and S. Song, "Appointed-time prescribed performance control for 6-DOF spacecraft rendezvous and docking operations under input saturation," *Aerosp. Sci. Technol.*, vol. 128, Sep. 2022, Art. no. 107744.
[20] P. Yang and Y. Su, "Proximate fixed-time prescribed performance tracking control of uncertain robot manipulators," *IEEE/ASME Trans. Mechatronics*, vol. 27, no. 5, pp. 3275–3285, Oct. 2022.
[21] X. Bu, B. Jiang, and Y. Feng, "Hypersonic tracking control under actuator saturations via readjusting prescribed performance functions," *ISA Trans.*, vol. 134, pp. 74–85, Mar. 2023.
[22] G. Wang, W. Yang, N. Zhao, Y. Shen, and C. Wang, "An approximation-free simple controller for uncertain quadrotor systems in the presence of thrust saturation," *Mechatronics*, vol. 72, Dec. 2020, Art. no. 102450.
[23] F. Wang, H. Gao, K. Wang, C. Zhou, Q. Zong, and C. Hua, "Disturbance observer-based finite-time control design for a quadrotor UAV with external disturbance," *IEEE Trans. Aerosp. Electron. Syst.*, vol. 57, no. 2, pp. 834–847, Apr. 2021.
[24] Y. Chen, J. Liang, Y. Wu, Z. Miao, H. Zhang, and Y. Wang, "Adaptive sliding-mode disturbance observer-based finite-time control for unmanned aerial manipulator with prescribed performance," *IEEE Trans. Cybern.*, vol. 53, no. 5, pp. 3263–3276, May 2023.
[25] L. Zhang, C. Wei, R. Wu, and N. Cui, "Fixed-time extended state observer based non-singular fast terminal sliding mode control for a VTVL reusable launch vehicle," *Aerosp. Sci. Technol.*, vols. 82–83, pp. 70–79, Nov. 2018.
[26] R. Li, Q. Zhu, H. Nemati, X. Yue, and P. Narayan, "Trajectory tracking of a quadrotor using extend state observer based U-model enhanced double sliding mode control," *J. Franklin Inst.*, vol. 360, no. 4, pp. 3520–3544, Mar. 2023.
[27] S. He, S.-L. Dai, Z. Zhao, T. Zou, and Y. Ma, "UDE-based distributed formation control for MSVs with collision avoidance and connectivity preservation," *IEEE Trans. Ind. Informat.*, pp. 1–12, 2023.
[28] S. He, S.-L. Dai, Z. Zhao, and T. Zou, "Uncertainty and disturbance estimator-based distributed synchronization control for multiple marine surface vehicles with prescribed performance," *Ocean Eng.*, vol. 261, Oct. 2022, Art. no. 111867.
[29] O. Doukhi and D. J. Lee, "Neural network-based robust adaptive certainty equivalent controller for quadrotor UAV with unknown disturbances," *Int. J. Control, Autom. Syst.*, vol. 17, no. 9, pp. 2365–2374, Sep. 2019.
[30] H.-P. Ren, S.-S. Jiao, X. Wang, and J. Li, "Adaptive RBF neural network control method for pneumatic position servo system," *IFAC-PapersOnLine*, vol. 53, no. 2, pp. 8826–8831, 2020.
[31] X. Shi, Y. Cheng, C. Yin, X. Huang, and S.-M. Zhong, "Design of adaptive backstepping dynamic surface control method with RBF neural network for uncertain nonlinear system," *Neurocomputing*, vol. 330, pp. 490–503, Feb. 2019.
[32] A. J. Al-Mahasneh, S. G. Anavatti, and M. A. Garratt, "Self-evolving neural control for a class of nonlinear discrete-time dynamic systems with unknown dynamics and unknown disturbances," *IEEE Trans. Ind. Informat.*, vol. 16, no. 10, pp. 6518–6529, Oct. 2020.
[33] H. Liu, G. Chen, and X. Tian, "Cooperative formation control for multiple surface vessels based on barrier Lyapunov function and self-structuring neural networks," *Ocean Eng.*, vol. 216, Nov. 2020, Art. no. 108163.
[34] G. Chen and Y.-D. Song, "Cooperative tracking control of nonlinear multiagent systems using self-structuring neural networks," *IEEE Trans. Neural Netw. Learn. Syst.*, vol. 25, no. 8, pp. 1496–1507, Aug. 2014.
[35] X. Wu, W. Zheng, X. Zhou, and S. Shao, "Adaptive dynamic surface and sliding mode tracking control for uncertain QUAV with time-varying load and appointed-time prescribed performance," *J. Franklin Inst.*, vol. 358, no. 8, pp. 4178–4208, May 2021.
[36] S. Shao and M. Chen, "Adaptive neural discrete-time fractional-order control for a UAV system with prescribed performance using disturbance observer," *IEEE Trans. Syst., Man, Cybern., Syst.*, vol. 51, no. 2, pp. 742–754, Feb. 2021.
[37] W. Zhang, X. Shao, W. Zhang, J. Qi, and H. Li, "Unknown input observer-based appointed-time funnel control for quadrotors," *Aerosp. Sci. Technol.*, vol. 126, Jul. 2022, Art. no. 107351.
[38] Y. Song, L. He, D. Zhang, J. Qian, and J. Fu, "Neuroadaptive fault-tolerant control of quadrotor UAVs: A more affordable solution," *IEEE Trans. Neural Netw. Learn. Syst.*, vol. 30, no. 7, pp. 1975–1983, Jul. 2019.
[39] C.-C. Hua, K. Wang, J.-N. Chen, and X. You, "Tracking differentiator and extended state observer-based nonsingular fast terminal sliding mode attitude control for a quadrotor," *Nonlinear Dyn.*, vol. 94, no. 1, pp. 343–354, Oct. 2018.
[40] V. K. Tripathi, S. C. Yogi, A. K. Kamath, L. Behera, N. K. Verma, and S. Nahavandi, "A disturbance observer-based intelligent finite-time sliding mode flight controller design for an autonomous quadrotor," *IEEE Syst. J.*, vol. 16, no. 1, pp. 1649–1660, Mar. 2022.
[41] Z. Zuo, B. Tian, M. Defoort, and Z. Ding, "Fixed-time consensus tracking for multiagent systems with high-order integrator dynamics," *IEEE Trans. Autom. Control*, vol. 63, no. 2, pp. 563–570, Feb. 2018.

[42] L. Wang and C. L. P. Chen, "Reduced-order observer-based dynamic event-triggered adaptive NN control for stochastic nonlinear systems subject to unknown input saturation," *IEEE Trans. Neural Netw. Learn. Syst.*, vol. 32, no. 4, pp. 1678–1690, Apr. 2021.
[43] H. Yang and D. Ye, "Adaptive fixed-time bipartite tracking consensus control for unknown nonlinear multi-agent systems: An information classification mechanism," *Inf. Sci.*, vol. 459, pp. 238–254, Aug. 2018.

HAITAO LIU (Member, IEEE) received the Ph.D. degree from the School of Mechanical and Automotive Engineering, South China University of Technology, Guangzhou, China, in 2012.

He is currently a Professor with the School of Mechanical Engineering, Guangdong Ocean University, Zhanjiang, China. His research interest includes the theory and applications of nonlinear control and robotics.

HONGJI ZHENG is currently pursuing the master's degree with Guangdong Ocean University, Zhanjiang, China.

His research interests include robust control, quadrotor UAV control, and nonlinear system control.

YUAN ZHANG received the master's degree from the School of Mechanical Engineering, Guangdong Ocean University, Zhanjiang, China, in 2015.

He is currently an Associate Researcher with the Agricultural Machinery Research Institute, Chinese Academy of Tropical Agricultural Sciences, Zhanjiang. His research interests include agricultural engineering, automatic control, and precise identification.

LIJIAO WEI received the master's degree from the School of Mechanical Engineering, Guangdong Ocean University, Zhanjiang, China, in 2015.

She is currently an Associate Researcher with the Agricultural Machinery Research Institute, Chinese Academy of Tropical Agricultural Sciences, Zhanjiang. Her research interests include agricultural engineering and agricultural informatization.